iScience

Article

Deciphering pre-existing and induced 3D genome architecture changes involved in constricted melanoma migration

Graphical abstract

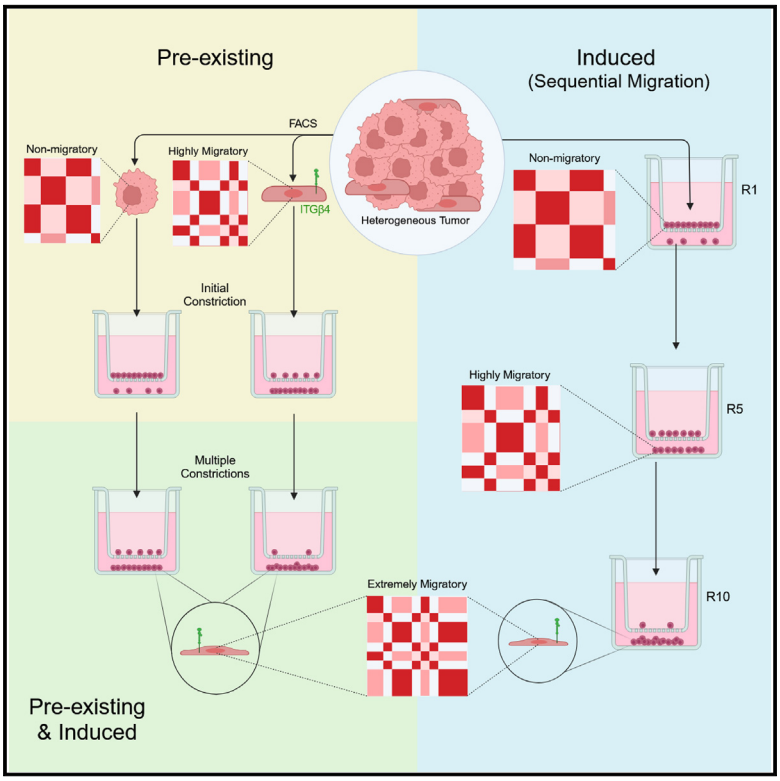

Highlights

- A375 ITGB4(+) cells migrate significantly better initially than ITGB4(-) cells
- Both selection and induction of ITGB4 are seen in sequentially migrated A375 cells
- Constricted migration causes similar compartment changes in ITGB4(+) and (-) cells
- Specific genomic regions are more prone to compartment changes following migration

Authors

Christopher Playter, Rosela Golloshi, Joshua H. Garretson, ..., Ahmed Saad, Samuel John Benson, Rachel Patton McCord

Correspondence

rmccord@utk.edu

In brief

Genomics; Cancer

Playter et al., 2025, iScience *28*, 112346
May 16, 2025
https://doi.org/10.1016/j.isci.2025.112346

CellPress

iScience

CellPress
OPEN ACCESS

Article

Deciphering pre-existing and induced 3D genome architecture changes involved in constricted melanoma migration

Christopher Playter,[1] Rosela Golloshi,[1,2] Joshua H. Garretson,[1] Alvaro Rodriguez Gonzalez,[3] Taiwo Habeeb Olajide,[1] Ahmed Saad,[1] Samuel John Benson,[1] and Rachel Patton McCord[1,4,*]

[1]Biochemistry & Cellular and Molecular Biology, University of Tennessee, Knoxville, TN 37996, USA
[2]Department of Cell Biology, Johns Hopkins School of Medicine, Baltimore, MD 21287, USA
[3]UT-ORNL Graduate School of Genome Science and Technology, University of Tennessee, Knoxville, TN 37996, USA
[4]Lead contact
*Correspondence: rmccord@utk.edu
https://doi.org/10.1016/j.isci.2025.112346

SUMMARY

Metastatic cancer cells traverse constricted spaces that exert forces on their nucleus and the genomic contents within. Cancerous tumors are highly heterogeneous and not all cells within them can achieve such a feat. Here, we investigated what initial genome architecture characteristics favor the constricted migratory ability of cancer cells and which arise only after passage through multiple constrictions. We identified a cell surface protein (ITGB4) whose expression correlates with increased initial constricted migration ability in human melanoma A375 cells. Sorting out this subpopulation allowed us to identify cellular and nuclear features that pre-exist and favor migration, as well as alterations that only appear after cells have passed through constrictions. We identified specific genomic regions that experienced altered genome spatial compartment profiles only after constricted migration. Our study reveals 3D genome structure contributions to both selection and induction mechanisms of cell fate change during cancer metastasis.

INTRODUCTION

Tumors are highly heterogeneous and only a subset of cells within the tumor possessess characteristics that make them more likely to successfully metastasize to secondary sites.[1,2] Metastasis involves a multi-step cascade that includes invasion through dense extracellular matrix (ECM), intravasation into the bloodstream, and extravasation to a secondary site.[3] During these steps, migrating cancer cells often must squeeze through spaces much smaller than the diameter of their nucleus, a process we refer to in this work as ''constricted migration''. Cells with an initial increased propensity for constricted migration may therefore selectively end up at the metastatic site. However, other alterations in cell phenotype may occur during the process of metastatic migration, as a result of exposure to different microenvironments and the physical forces on the cells as they squeeze through tight constrictions. In some cases, metastatic tumors have been found to contain both ''leader'' and ''follower''-type cells, in which the pre-existing cellular properties of the leaders are selected for, but further changes can occur in follower cells as they are exposed to new microenvironments.[4] These features of initial heterogeneity and environment-induced changes can be observed in cell culture models of cancer as well. As examples of heterogeneity, numerous different cancer cell lines in culture have been shown to contain stable subpopulations of stem-like cells[5,6] or other subtypes that are marked by the expression of certain proteins.[7,8] The A375 human melanoma cell line, which is the focus system in this study, has previously been found to exhibit heterogeneity and the potential for multiple subpopulations with different metastatic capacities in mice[9] and *in vitro* migration experiments.[10] In addition to cellular differences created by this initial cellular heterogeneity, external stresses such as physical forces applied on cells or alterations to substrate stiffness can further alter cellular phenotypes and epigenetic marks.[11–13]

For better diagnostics and treatment, it is key to develop an understanding of which cellular features pre-exist and increase a cell's initial propensity to migrate and to distinguish these factors from further changes that happen during metastatic migration and influence the cancer cell's aggressiveness at a secondary site. Distinguishing these features is difficult, however, given the complex combination of selection from a heterogeneous population as well as induced alterations that occur in metastasis as discussed above. Emerging evidence has identified nuclear architecture and 3D genome structure as a potential key factor in cancer progression and metastasis. Genome wide chromosome conformation capture (Hi-C) experiments across multiple cancer types have identified changes in spatial genome organization patterns that correlate with cancer progression, epithelial to mesenchymal transition, and metastasis.[14–18] In particular, alterations in cancer phenotype are often associated with changes in the spatial compartmentalization of chromosome regions into active (A) and

inactive (B) compartments.[19] This spatial separation of typically euchromatic (A) and heterochromatic (B) genomic regions, which is accomplished through phase separation-type interactions and tethering to nuclear structures like the lamina, can influence gene regulation and help maintain cell fate.[19] Therefore, alterations to A and B compartmentalization in cancer progression may contribute to alterations in cell phenotype and changes to the expression of genes involved in cancer progression.[16] However, these previous studies have not been able to determine which of these "progression associated 3D genome changes" could have pre-existed in a subpopulation of cells and been selected for and which changes could be induced during the process of metastasis.

Many questions also remain about how migration-favoring initial states or induced alterations are encoded. There is evidence that both initial heterogeneity and changes induced by stresses could be encoded by patterns of gene expression and epigenetic chromatin modification changes. Subtypes of breast cancers and B cell neoplasms are characterized by differences in 3D genome structure.[18,20] Computational models suggest that 3D chromosome folding into spatial compartments can help encode stable memories of epigenetic states,[21] potentially maintaining subpopulation identity across cell generations. Meanwhile, in terms of induced changes, passage through multiple constrictions in a microfluidic device was shown to increase the histone modification H3K27me3 and decrease H3K9ac in HT1080 cells.[22] Such histone modifications can contribute to the spatial compartment organization of chromosomes.[19] Here, we investigate both what chromosome structures are associated with initial migration ability, and which are specifically changed only after passage through constrictions.

Previously, we have found that human melanoma cells (A375) that have passed through ten rounds of constricted migration exhibit stable differences in migratory phenotype, gene expression, nuclear architecture, and 3D genome structure.[10] Our previous results could not fully distinguish whether these changes were the result of selection on an initially heterogeneous population or the result of constriction-induced changes. We found that new populations of cells grown from individual clones of the parental A375 cell population underwent similar changes after sequential constricted migration. However, it is known that cancer cells can regenerate heterogeneity as they divide,[23] so the changes with constricted migration in the clonal populations could still be in part due to selection. Here, we identify a cell surface protein, integrin-β4 (ITGB4), as a marker whose RNA and protein expression level closely associates with A375 constricted migration proficiency. ITGB4 is the beta subunit of a heterodimeric receptor for extracellular matrix components and select cell adhesion molecules with the preferred binding partner integrin Alpha-6.[24] This protein has often been discussed in previous literature for its potential role in metastatic propensity, though depending on the cancer type and context, high ITGB4 levels may be a migration-favoring[25–28] or inhibiting factor.[29] Overall, an increase in ITGB4 expression tends to associate with poor prognosis for a majority of cancers.[29] ITGB4 is currently used as a prognosis marker for both pancreatic[25] and lung cancers.[30] ITGB4's role in melanoma is less well understood, but some results have indicated an increase in its expression in skin cancer tumors.[31] We find that cells within the parental A375 population with higher ITGB4 expression (ITGB4[+]) initially migrate at a higher efficiency through 5 μm pores, a pore size that substantially constricts the cell nucleus. By isolating ITGB4(+) cells from the parental A375 population, we can identify pre-existing cellular characteristics and 3D genome structures that favor migration. Additionally, we find key differences between ITGB4(+) cells and cells that have passed through 10 rounds of constriction (Bottom10). By using this model, we can tease apart pre-existing 3D genome structures that enable constricted migration and 3D genome structures that arise as a result of constricted migration.

RESULTS

ITGB4 expression is increased following A375 constricted migration and is associated with higher initial migration rates

Our previously published RNA-seq data[10] for A375 cells that had passed through 10 rounds of 5 μm constrictions revealed over 1000 differentially expressed (DE) genes (867 up and 626 down) following constricted migration (Bottom10) when compared to unmigrated cells (parental) (Figure 1A). Of the most upregulated genes, integrin-β4 (ITGB4), in particular stood out as a potentially useful cell surface marker that would enable sorting and tracking of cells and as a protein which had previously documented involvement in increasing cancer metastasis. We found that this upregulation occurs in constricted cells only, not when A375 cells migrate through 12 μm pores that exert much less deformation on the nucleus (Figure 1B). Thus, increased ITGB4 gene expression cannot be an effect of one of the other factors common to migration such as fibronectin or serum gradient exposure. We further found that surface protein levels of ITGB4, as measured by flow cytometry (see STAR Methods), increased after 10 rounds of constricted migration not only in the parental population, but also in A375 populations grown from four isolated individual cells (clonal populations 1–4) (Figure 1C). This shows that rather than an ITGB4 expressing cells only being a static subset of the parental A375 cell line, high levels of this protein can result from constricted migration even in different clonal lines. Since ITGB4 is expressed on the cell surface, we were able to use fluorescence-activated cell sorting (FACS) to isolate cells that highly expressed ITGB4 from the parental population, resulting in a subgroup we term ITGB4(+), as well as cells that had almost no ITGB4 surface expression, which we call ITGB4(−).We isolated ∼20% of parental cells as ITGB4(+) and ∼35% as ITGB4(−) (Figure 1D). The ITGB4(+) cells maintained high ITGB4 expression over rounds of cell division, even across 7 weeks of growth (Figure S1A). We found no proliferative differences between our ITGB4(+) or ITGB4(−) cells (Figure S1B).

We next challenged these ITGB4(+) and ITGB4(−) cells to migrate through 5μm pore Transwell filters to test their initial migratory ability. We found that the ITGB4(+) cells migrated at a significantly higher rate than ITGB4(−) cells (Figure 1E). In fact, the ITGB4(+) cells migrated about as well as parental cells after 10 rounds of constriction (Bottom10). This raises the question: is the ITGB4(+) sub-population the group that is being

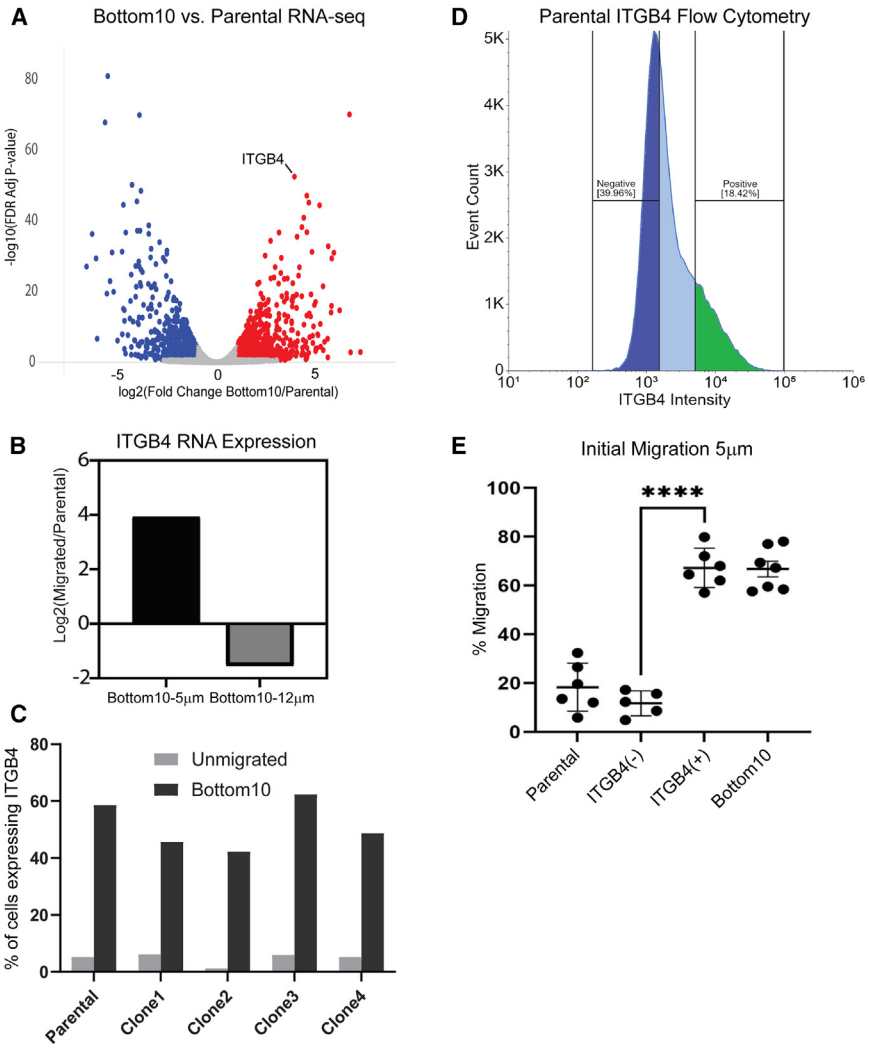

Figure 1. ITGB4 expression is increased following A375 constricted migration and is associated with higher initial migration rates

(A) RNA-seq analysis of all genes comparing Bottom10 vs. parental cells. Significantly upregulated (red) or downregulated (blue) and unchanged (gray) genes are shown. Thresholds are log2FC > 1 and adj. p-val. <0.01. ITGB4 labeled.

(B) ITGB4 log2(migrated/parental) RNA levels after 10 rounds migration through 5 μm (constricting) and 12 μm (non-constricting) pores.

(C) Flow cytometry measured percentage of cells that express surface ITGB4 protein for parental and all 4 clonal populations before migration and after 10 rounds of sequential migration.

(D) ITGB4 intensity plot (based on green fluorescent antibody labeling) used to FACS sort ITGB4(−) cells (*dark blue)* and ITGB4(+) cells (*green).* Cells in the light blue section were not collected.

(E) The initial migration rates (% of cells that migrated through pores) through 5 μm Transwell pores for parental, ITGB4(−), ITGB4(+) cells along with the final migration rate for Bottom10 cells. All biological replicates shown, with mean and standard deviation shown as line and whiskers. (****p = <0.0001, two-tailed t test).

selected by rounds of constriction and thus isolated as Bottom10 cells at the end of sequential constrictions? Thus, we further characterized ITGB4(+) phenotypes in comparison to ITGB4(−) and Bottom10 cells.

ITGB4(+) cells exhibit phenotypic differences that represent an intermediate between ITGB4(−) and sequentially constricted Bottom10 cells

Cells that express ITGB4 exhibit morphological differences compared to ITGB4(−) cells. ITGB4(−) cells had a more epithelial morphology, whereas ITGB4(+) cells exhibited fewer cell-cell adhesions and were more likely to extend reaching protrusions similar to Bottom10 cells (Figure 2A). However, the growth of these cell populations on a 2D surface also provided a first indication that ITGB4(+) cells were not quite the same as Bottom10 cells. Quantifying the percentage of cells with extended protrusions showed that ITGB4(+) cells had a significantly higher percentage of cells with protrusions (white arrows in 2A) compared to ITGB4(−) cells, but not as many as Bottom10 cells (Figure 2B). The cell body aspect ratio across the imaged cells is similar between ITGB4(+) and ITGB4(−) and both were significantly less elongated than Bottom10 cells (Figure 2C). Nonetheless, ITGB4(+) cells showed increased wound healing, similar to that of Bottom10 cells, in a 2D scratch assay compared to the ITGB4(−) cells, which showed very little wound closure even after 24 h (Figure 2D, Videos S1, S2, and S3). After seeing the differences between these cell groups in a 2D environment, we next asked if they behaved differently when embedded in a 3D collagen matrix. Cells were embedded in a 3D collagen matrix (see STAR Methods) and allowed to acclimate for 96 h. Again, there were visually apparent differences between ITGB4(−) and ITGB4(+) cells (Figure 2E). ITGB4(−) cells remained spherical and failed to migrate through the matrix, instead rotating in place. ITGB4(+) cells, however, grew extremely long protrusions through the collagen matrix. These protrusions were similar to those exhibited by Bottom10 cells placed in a collagen matrix, but while Bottom10 cells also deformed their nuclei and translocated through the matrix,[10] ITGB4(+) cells did not show net movement through the matrix. (Figure 2E, Videos S4 and S5 (ITGB4-), Videos S6 and S7 (ITGB4+), Video S8 (Bottom10)).

ITGB4 expression increase across successive rounds of migration shows both selection and induction features

To further investigate to what extent sequential constriction selects for high ITGB4 expressing cells due to their initially high migration efficiency, we next monitored in detail the levels of ITGB4 cell surface expression across the rounds of constricted

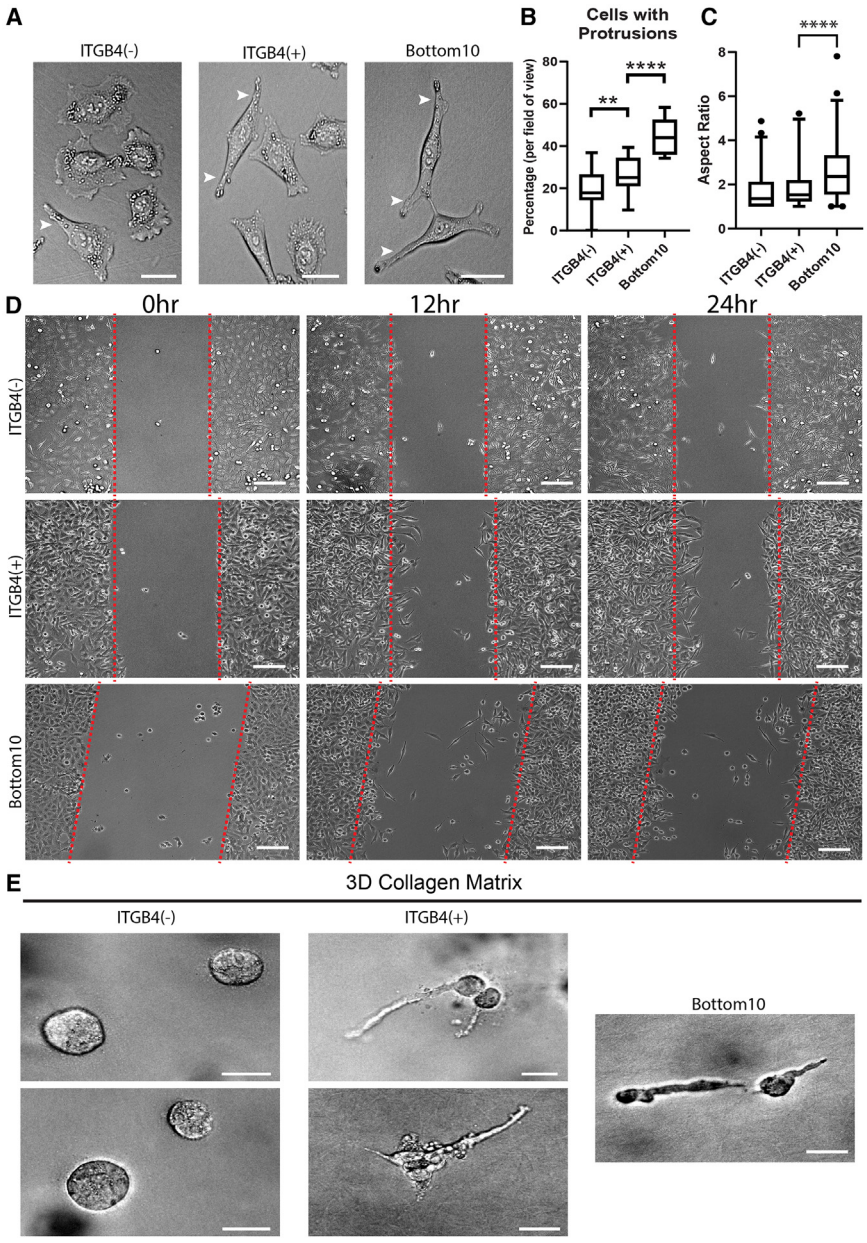

Figure 2. ITGB4(+) cells exhibit phenotypic differences that represent an intermediate between ITGB4(−) and sequentially constricted Bottom10 cells

(A) 2D phase contrast images of ITGB4(−), ITGB4(+), and Bottom10 A375 cells. Scale, 70 μm. Protrusions indicated by white arrows.

(B) Quantification of the percentage of cells that have protrusions for ITGB4(−), ITGB4(+), and Bottom10 cells per field of view. Images taken at 20x on EVOS. Total cells counted: 695-ITGB4(+), 559-ITGB4(−), 468-Bottom10. (**p = 0.0048, ****p < 0.0001, two-tailed t test).

(C) Aspect ratio quantification (major axis length/minor axis length) for ITGB4(−), ITGB4(+), and Bottom10 A375 cells. (****p < 0.0001, two-tailed t test) N = ∼100 cells/condition. Boxplots in B and C show minimum, 25th %ile, median, 75th %ile and maximum.

(D) Scratch assay images (20x, phase contrast) at 0, 12, and 24 hr post scratch for ITGB4(−), ITGB4(+), and Bottom10 cells. Red dashed lines mark initial scratch location throughout time lapse. See Videos S1, S2, and S3. Scale, 300 μm.

(E) 40x Phase contrast images of ITGB4(−), ITGB4(+), and Bottom10 cells embedded in 3D collagen matrix 96 h post seeding. See Videos S4, S5, S6, S7, and S8. Scale, 70 μm.

migration, starting with the parental cell population. If cells expressing ITGB4 are enriched by each round of migration, we would expect an increase in the percentage of ITGB4 expressing cells found immediately after each round of migration compared to just before migration. Using flow cytometry, we determined the percentage of cells that highly expressed ITGB4 before and after each round of 10 sequential rounds of migration through 5 μm Transwell pores (Figure 3A). This experiment allowed us to monitor ITGB4 expression in 3 different settings: constricted migration (5 μm), non-constricted migration (12 μm), and no migration at all (No Well).

Previous work has shown that cell surface integrin expression can be influenced by cell growth conditions such as confluence and starvation.[32,33] We found that in A375 cells, ITGB4 protein expression on the cellular surface was increased additively by both cell confluency and media depletion (Figures S1B–S1D). Therefore, we carefully normalized our ITGB4 expression results across sequential migration by the "No Well" control, which mimicked the same confluence and media conditions at all timepoints, but without any migration. During the sequential migration, both the parental population and the cells derived from a single A375 clone (Clone3) showed an increase in ITGB4 surface protein expression level as they progressed through more rounds of migration (Figures 3B and 3C). Importantly, the increase was specific to constricted migration (not observed in the 12 μm pore experiment), indicating that other conditions such as exposure to fibronectin did not cause the increase. In some rounds of migration (see stars in Figures 3B and 3C), we saw the expected signature of selection, where ITGB4(+) cells increased immediately after cells were passed through the Transwell. However, in other rounds of migration, this was not the case: instead, cells increased ITGB4 levels during growth after migration (see crosses, Figures 3B and 3C). This provides evidence of both selections from the previous population and some other mechanism of further ITGB4 induction after constricted migration. We also carried this experiment out on ITGB4(+) and ITGB4(−) cells (Figure S2) and saw instances of both selection and induction, but not to the same magnitude as seen in our parental or clone populations.

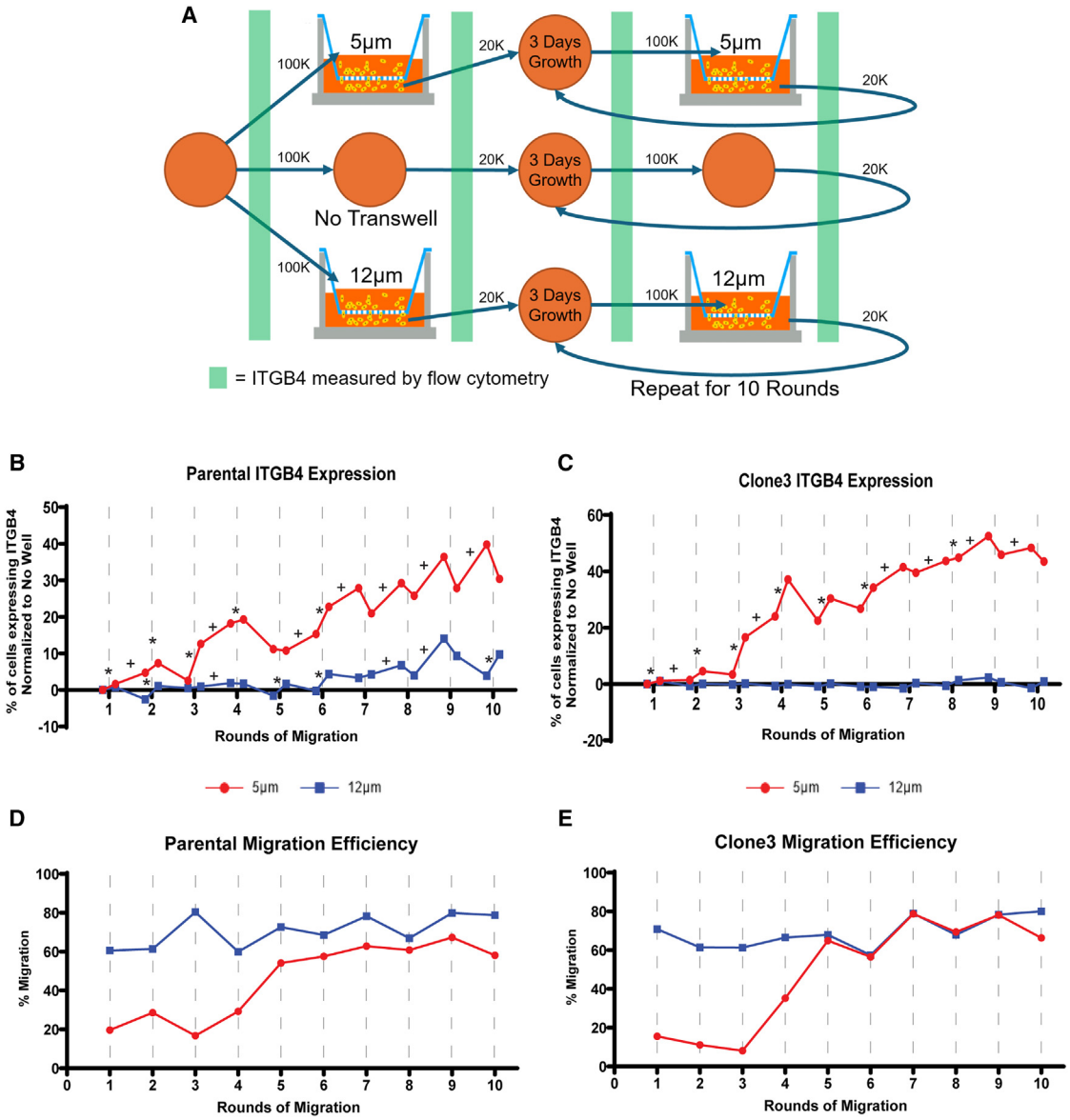

Figure 3. ITGB4 expression increase across successive rounds of migration shows both selection and induction features

(A) Experimental approach to monitor ITGB4 surface expression across rounds of constricted migration. Orange circles represent culture dishes. For all conditions, 100K cells were always used to start the Transwell experiment, and 20K cells taken for the subsequent 3 days growth.

(B) ITGB4 surface protein expression (flow cytometry) over sequential rounds of migration for 5 μm, *red*, and 12 μm, *blue*, Transwell pores normalized to the no well condition. Vertical dashed lines represent a single Transwell migration event. Stars indicate selection-like increase after Transwell passage, while crosses indicate further induction during growth.

(C) Clone3 ITGB4 surface protein expression (flow cytometry) over sequential rounds of migration. All colors and symbols as in (B).

(D) Parental migration rates (% of cells that migrated through pores) for 5 μm, *red*, and 12 μm, *blue*, pores throughout the 10 rounds of sequential migration matching the flow cytometry data conditions in (B).

(E) Clone3 migration rates matching the 10 rounds of sequential migration matching the conditions in (C).

Across rounds of sequential migration, the migration rate at each round correlates well with the ITGB4 expression both before the Transwell (0.823, 0.927, Pearson's R) and the ITGB4 expression measured immediately after migration (0.770, 0.874) for parental and Clone3 cells, respectively (Figures 3D and 3E). Specifically in the round 3–5 range, both ITGB4 expression and migration ability exhibit large increases. Again, if passage through the Transwell filter simply selected for ITGB4 expressing cells, we would expect that the 20% of cells that migrate in the first round (Figures 3D and 3E) would all have high levels of ITGB4 expression. Instead, we see that it actually takes several rounds of migration to produce the substantial increase in both ITGB4 expression and

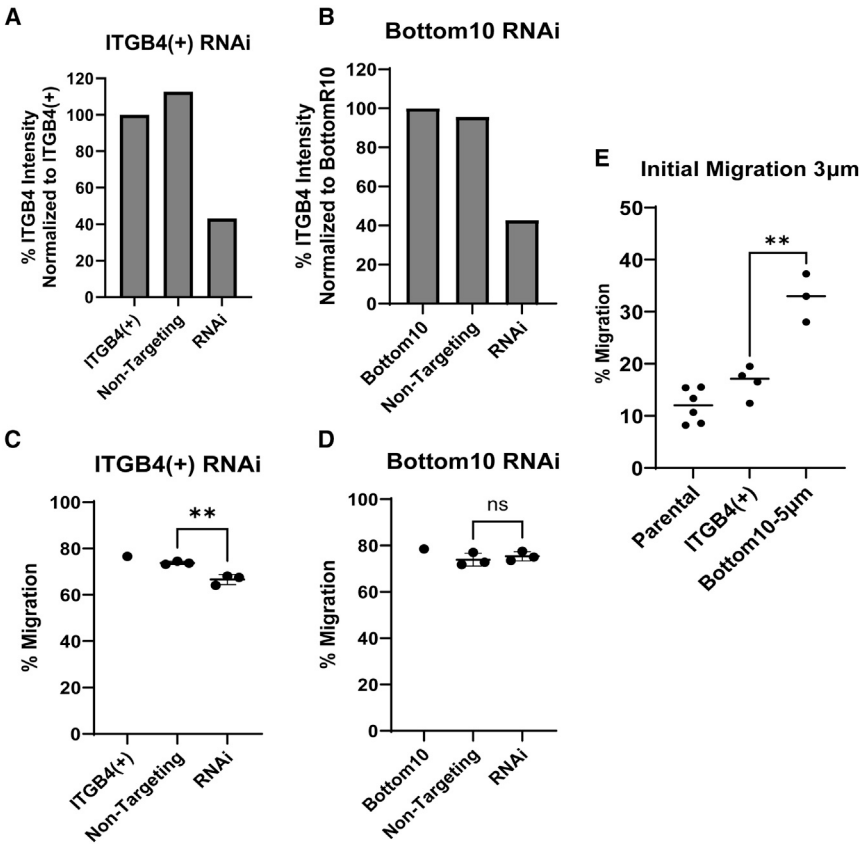

Figure 4. Knockdown of ITGB4 alters migration ability of previously unmigrated cells

(A) Bar plot quantifying ITGB4 surface protein expression levels (flow cytometry) for untreated ITGB4(+) cells compared to those given non-targeting control RNAi, and ITGB4 RNAi for 96 h. A single biological replicate is shown, with two more independent biological replicates shown in Figure S3.

(B) ITGB4 surface protein expression in control and RNAi knockdown of Bottom10 cells, conditions as in (A). A single biological replicate is shown, with two more independent biological replicates shown in Figure S3.

(C) Migration rates (% of cells that migrated through 5 μm pores) for conditions in Figure 4A. Three biological replicates for non-targeting and ITGB4 RNAi are shown (**p = 0.0055, two tailed t test). Additional biological replicates corresponding to independent RNAi knockdown experiments are shown in Figure S3.

(D) Migration rates for conditions in Figure 4B through 5 μm Transwell pores. (ns = $p > 0.05$, two tailed t test). For C and D, all data points are shown with mean ± SD indicated.

(E) Initial migration rates for parental, ITGB4(+), and Bottom10 cells when challenged with 3 μm Transwell pores. (**p = 0.0024, two tailed t test) Biological replicates shown. All data points shown with mean indicated.

migration efficiency. Together, the data suggest that ITGB4 can be an initial selection marker for migratory cells, but can also be further increased in the cell population as a result of migration.

Knockdown of ITGB4 alters migration ability of previously unmigrated cells

The strong correlation between ITGB4 expression and constricted migration proficiency raised the question: is ITGB4 presence on the cell surface needed for effective constricted migration? To test this, we knocked down the expression of ITGB4 using RNAi in both ITGB4(+) and Bottom10 cells. By flow cytometry, we found that RNAi decreased cell surface ITGB4 expression by 60% in both cell populations (Figures 4A and 4B). However, we found that this ITGB4 reduction affected constricted migration rates only in the previously unmigrated ITGB4(+) cell population. In these cells, reducing ITGB4 levels decreases constricted migration rates moderately, but significantly (Figures 4C and S3). In contrast, the Bottom10 cells, which also have high ITGB4 levels initially, but have already passed through 10 rounds of constriction, exhibited no migration difference following knockdown of ITGB4 expression (Figures 4D and S3). Thus, ITGB4 expression is more important to the migration ability of cells that have not previously passed through constrictions.

Combined with the phenotypic differences observed between ITGB4(+) and Bottom10 cells in Figure 2, this result points to additional phenotypic changes that happen as a result of sequential constricted migration that are not present in an initially highly migratory subpopulation. Further supporting this idea, we found that while ITGB4(+) cells migrated through 5 μm pores at similar rates as Bottom10 cells, when we challenged both cell groups to migrate through even smaller 3 μm pores, we found that Bottom10 cells migrated at significantly higher rates than ITGB4(+) cells (Figure 4E). This suggests that having experienced the stress of 5 μm pores aided the Bottom10 cells' ability to pass through the tighter constrictions, which involve even greater nucleus deformation.

3D genome structure differences exist between ITGB4(+) and ITGB4(−) cells at the compartment level

Based on the combination of migration ability and the morphological differences we saw between our ITGB4(+) and ITGB4(−) cells, we next asked if they also had altered 3D genome structures that associated with such differences. Genome wide chromosome conformation capture (Hi-C) was carried out on ITGB4(+) and ITGB4(−) cells sorted from both the parental and one Clonal population. Using principal component analysis, the first eigenvector (PC1) for each 250 kb region for all individual chromosomes represents the A/B compartmentalization profile for each condition. We found that these compartment profiles were highly correlated between biological replicates obtained from two independent sorts of ITGB4(+) and (−) populations from parental cell cultures. Replicate compartment profiles show Pearson's correlation coefficients of 0.95 and 0.97 for ITGB4(+) and (−) respectively. We found consistent differences

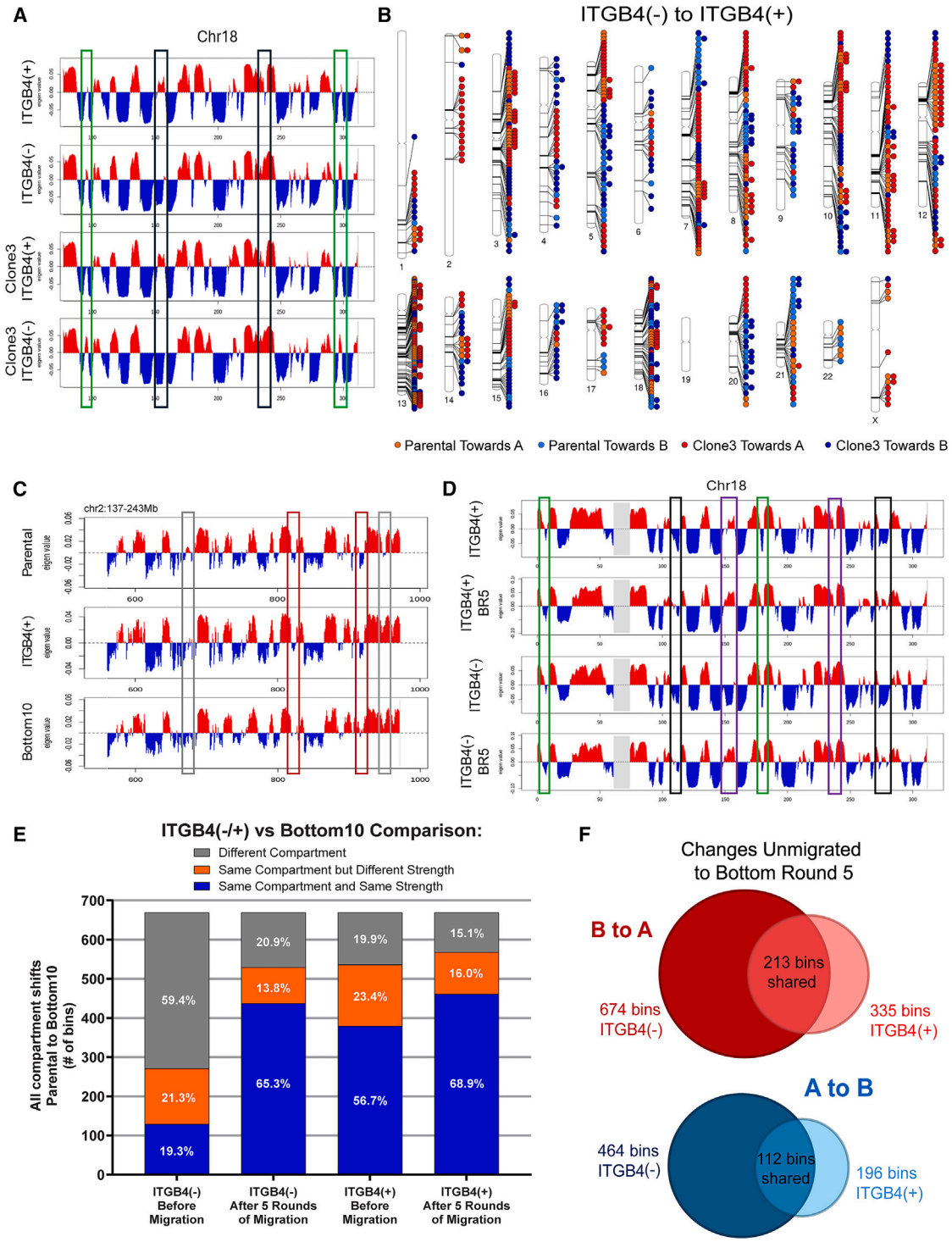

Figure 5. 3D Genome structure differences exist between ITGB4(+) and ITGB4(−) cells at the compartment level and are further altered following constricted migration

(A) 250 kb binned compartment tracks of the right arm of Chr18 for both parental and Clone3 ITGB4(+) and ITGB4(−) cells. Black boxes outline compartment regions which are switched between conditions. Green boxes outline compartment regions where strong shifts in compartment strength exist between conditions.

(legend continued on next page)

in compartmentalization between ITGB4 expressing and non-expressing cells (Figure S4A). Chr18 for example, had regions of compartment switches between ITGB4(+) and ITGB4(−) cell conditions (Figure 5A black boxes). We also found instances of compartment shifts between ITGB4(+) and ITGB4(−) cell conditions where compartment strength had been altered between the cells (Figure 5A green boxes). Examples of compartment differences on other chromosomes can be found in Figures S4B–S4F. To see how many genomic regions shift toward the A compartment or B compartment on a more global scale, we compiled every 250 kb region that had a 20% shift in eigenvector value in either direction and plotted them on a phenogram[34] (Figure 5B). This phenogram then showed us the position and direction of every compartment shift for both parental and Clone3 cells when comparing ITGB4(−) to ITGB4(+) cells. While there are hotspots where shifts occur more frequently, nearly every chromosome had some region that shifted compartments. We found many areas where parental and Clone3 shifts were concordant, and though not all changes were observed in both cell groups, no regions changed in opposite directions in parental vs. Clone3 ITGB4(+) cells. This indicates that, overall, there is a consistent 3D genome compartment pattern that characterizes the initially migratory ITGB4(+) subpopulation.

The 3D genome structure of ITGB4(+) cells is an intermediate state between parental and Bottom10 cells

Morphologically and functionally, our results thus far have revealed the ITGB4(+) cells from the unmigrated population share some but not all characteristics of sequentially migrated Bottom10 cells. Our observation that ITGB4(+) cells exhibit 3D genome compartment differences from ITGB4(−) next led us to ask whether these are the same alterations we had previously observed in Bottom10 cells after sequential migration.[10] Therefore, we used our Hi-C data to identify regions of the genome where ITGB4(+) cells had the same compartment identity as Bottom10 cells (Figure 5C gray boxes) or the same compartment identity as unmigrated parental cells (Figure 5C red boxes). Finding examples of similarities to both parental and Bottom10 cells suggested that, while some features of the ITGB4(+) genome structure before migration could be selected for and thus observed in Bottom10 cells, there were other portions of the genome structure that changed only after constricted migration.

ITGB4(+) and ITGB4(−) cells are sensitive to constricted migration and resemble Bottom10 cells more closely following multiple rounds of migration

We allowed ITGB4(+) and ITGB4(−) cells to migrate through 5 rounds of 5 μm constrictions. Afterward, we collected the cells for Hi-C analysis to determine what genomic regions have altered compartmentalization after migration and if these changes are similar to those observed after constricted migration of the parental population. Indeed, we found that both ITGB4(+) and ITGB4(−) cells had altered compartmentalization at the same locations in the same direction following constricted migration on multiple chromosomes (Figure 5D; Figures S4G–S4J) where black boxes show regions with compartment switches and green boxes show regions of strong compartment strength shifts that occurred following constricted migration. The purple box shows a region where ITGB4(+) cells show a shift after migration where the ITGB4(−) cells show a compartment switch coinciding.

We then quantified the compartment profile similarity between Bottom10 cells and ITGB4(+) or ITGB4(−) cells before and after they underwent constricted migration (Figure 5E). As parental cells went through sequential constricted migrations to become Bottom10 cells, 669 bins (250 kb resolution) shifted in their compartment identity. When looking at ITGB4(−) cells prior to migration, only 271 of these 669 Bottom10-specific bins were already in the same compartment as Bottom10. There is a wide range of values that count as being in the "same compartment", even though the compartment strength may be dissimilar, so we added another level of specificity to ask which bins matched in compartment strength (eigenvector values within 10% of each other). We find that of those 271 bins that already matched the compartment identity of Bottom10 before ITGB4(−) cells were migrated, only 129 were also similar in compartment strength to Bottom10. After the ITGB4(−) cells went through 5 rounds of constricted migration, however, an additional 258 bins (529 total) switched into the same compartment as Bottom10 cells, and the number of bins with similar compartment strength grew by 308 bins (437 total). ITGB4(+) cells before migration were more similar to Bottom10 cells compared to ITGB4(−) cells: 536 of the 669 Bottom10-specific bins were already in the same compartment and 379 of them were also of similar compartment strength. And, as with ITGB4(−) cells, following migration, ITGB4(+) cells became even more similar

(B) Phenogram showing all compartment shifts (change in eigenvector1 value >0.04 for toward A or < −0.04 for toward B) between ITGB4(−) and ITGB4(+) cells for both parental and Clone3 populations. Each circle represents a single 250 kb bin that is shifted, and its location is marked by a line to its respective chromosome. Regions with 2 circles side by side show shifts found in both populations.

(C) 250 kb binned compartment track of a section of Chr2 for parental, ITGB4(+), and Bottom10 cells showing that ITGB4(+) cells share regions with both unmigrated and migratory populations. Red boxes show regions where ITGB4(+) and parental show similar compartment identity and differ from Bottom10. Gray boxes show regions where ITGB4(+) and Bottom10 show similar compartment identity and differ from parental.

(D) 250 kb binned compartment tracks of Chr18 for ITGB4(+) and ITGB4(−) cells before and after 5 rounds of migration. Black boxes highlight regions where compartment switches have occurred in both conditions following migration. Green boxes highlight regions where strong compartment shifts have occurred in both conditions following migration. Purple boxes highlight regions where ITGB4(−) compartment switch after migration to match ITGB4(+) before and after migration.

(E) Bar plot comparing compartment identity of ITGB4(−) and ITGB4(+) cells before and after migration to compartments that are altered between parental and Bottom10 cells. Cells following migration have more regions that are similar to Bottom10 cells than before migration.

(F) Venn diagrams of the number of bins that switch after migration in both ITGB4(+) and ITGB4(−) toward both A and B compartments. Many of the same bins switch with migration for both initially ITGB4(+) or ITGB4(−) cells. Individual compartment profile plots (A–D) are from Hi-C replicate 2 (a more stringent sort) while global comparisons (E and F) use compartment profiles that were averaged between Hi-C replicates.

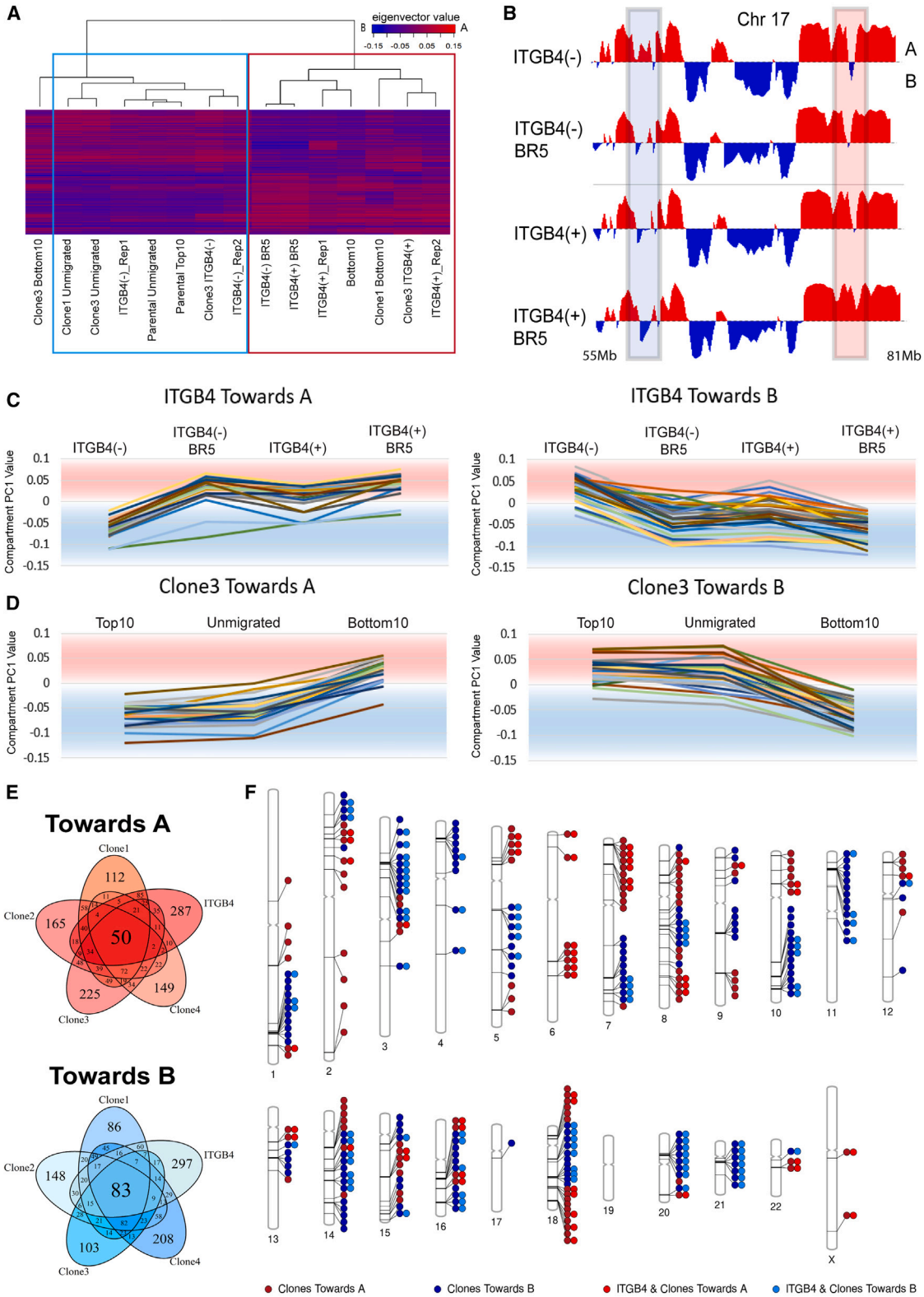

(legend on next page)

to Bottom10 cells as the number of bins in the same compartment increased by 32 (568 total) and an additional 82 bins (461 total) reached the same compartment strength as Bottom10.

When we only looked at compartment switches that occurred following constricted migration of both ITGB4(+) and ITGB4(−) cells, we found that while more changes occurred after ITGB4(−) cells had undergone constrictions, many constriction-associated switched regions are shared between ITGB4(+) and ITGB4(−) cells (Figure 5F). This suggests that the act of passing through constrictions plays a pivotal role in altering the 3D genome even of already highly migratory cells and that the final 3D genome state of cells after sequential migration involves both selecting for properties already inherent to certain subpopulations of cells and further inducing alterations during the rounds of migration.

Specific regions of the genome are more prone to compartment shifts/switches following constricted migration

We clustered all cellular conditions according to compartment signatures (Figure 6A). In general, migratory cell conditions (red box) clustered together and separately from non-migratory conditions (light blue box). Notably, the most similar compartment profiles were found between the ITGB4(+) and ITGB4(−) cells that had migrated through 5 rounds of constriction. This suggests that even though ITGB4(−) and (+) cells start out with distinct compartment profiles, constricted migration shifts their compartment profiles to become very similar. We found that if we arrange conditions from least to most migratory (from poorly migratory ITGB4(−) cells to ITGB4(+) cells that had been migrated 5 times), we can see genomic regions which progressively shift compartments (Figure 6B). Shown in the blue box is an example where a strong A compartment shifts to a strong B compartment as the cells become more migratory. Just downstream, the red box highlights a shift in the opposite direction, where a strong B compartment shifts to becoming a strong A compartment. In each case, we observed that ITGB4(+) cells often already looked more similar to migrated ITGB4(−) cells but then passage through constrictions of this already migratory population resulted in even further compartment shifts in the same direction as the migrated vs. unmigrated ITGB4(−). This trend was observed over many regions genome-wide. We identified regions that progressively shifted their compartment from ITGB4(−) to ITGB4(−)BR5 to ITGB4(+) to ITGB4(+)BR5 cells by calculating the slope of the eigenvector across these conditions and identifying regions where the slope (positive or negative) was greater than 1.5 standard deviations from the mean. This analysis revealed 668 regions that progressively shift toward A and 640 regions that progressively shift toward B (the top 30 most dramatic slopes are shown in Figure 6C).

Our next goal was to determine the genomic regions that are the most susceptible to compartment shifts or switches following constricted migration. Previously, we had completed Hi-C on four different clonal populations at 3 different conditions: Top10 (unable to migrate though given 10 chances), unmigrated, and Bottom10. We ordered these conditions from least to most migratory and using their eigenvector values for each 250 kb region were able to calculate a slope for each region. In the same way that we did for the ITGB4 spectrum, we considered regions with a positive or negative slope greater than 1.5 standard deviations from the mean as shifted regions following constricted migration (top 30 most positive and negative sloped bins shown in (Figure 6D; Figure S5). Once we found which bins were the most susceptible to shifts during each clonal and ITGB4 progressions, we identified bins that overlapped across all conditions. Across all clonal and ITGB4 progressions, 50 total 250 kb bins shifted toward the A compartment and 83 total bins shifted toward the B compartment (Figure 6E). If we only consider the clonal progressions, those numbers increase to 122 bins toward A and 165 bins toward B. The shifts shared by clonal populations but not the ITGB4 spectrum likely reflect the different initial starting state of ITGB4-sorted cells. We next investigated the genomic locations of these compartment shifts by plotting all the shifting regions on a phenogram (Figure 6F). We found that constriction-sensitive regions are located throughout the genome with all but chromosome 19 having at least one shifted region. Most chromosomes have regions that shift both toward the A and the B compartments. We observed hotspot areas, where specific chromosomes had larger regions that were sensitive, suggesting that these areas could be at play in enabling better migration, i.e., chromosome 3, 11, and 18. In particular, comparing chr17, chr18, and chr19, we note that chr18 experiences far more changes. Chromosomes 17 and 19 are gene rich and internally localized while chromosome

Figure 6. Specific regions of the genome are prone to compartment shifts/switches following constricted migration making all migratory cells more similar to each other

(A) Clustering analysis using the 200 most variable 250 kb compartment bins. Light blue box: non-migratory cell conditions. Red box: migratory cell conditions.

(B) PC1 compartment profiles for chr17:55–81 Mb for ITGB4(−), ITGB4(−)BR5, ITGB4(+), and ITGB4(+)BR5 conditions ordered from least to most migratory (top to bottom). Blue box = progressive shift in compartment identity toward a stronger B compartment as migration ability increases. Red box = progressive shift toward a stronger A compartment as migration ability increases.

(C) The top 30 250 kb binned regions with positive slopes (toward A) and negative slopes (toward B) as cells increase migration ability. Each bin's compartment value (PC1) is plotted for ITGB4(−), ITGB4(−)BR5, ITGB4(+), and finally ITGB4(+)BR5 and tracked from left to right.

(D) The top 30 250 kb binned regions with positive slopes (toward A) and negative slopes (toward B) as cells increase migration ability for Clone3 cells. Each bin's compartment value is plotted for Top10, unmigrated, and Bottom10 cells and tracked from left to right. Other clonal populations can be found in Figure S3.

(E) 5-way Venn diagram showing the number of 250 kb bins that shift toward A or toward B across either ITGB4 conditions or clonal migration. All bins that have slopes +/− 1.5STD from the mean slope are included. The number on the outer most part of ovals represents the number of bins that are specific to each condition. The number in the center represents the number of bins that are shared across all 5 conditions.

(F) Phenogram showing locations of all shifted 250 kb bins shared between the 4 clonal populations (dark red and dark blue) and bins that are shared between the clonal populations and the ITGB4 conditions (light red and light blue). Each circle represents a single 250 kb bin that has shifted. Single circles show bins only changed across the 4 clonal populations, whereas double circles show regions where the ITGB4 conditions also shared that shift.

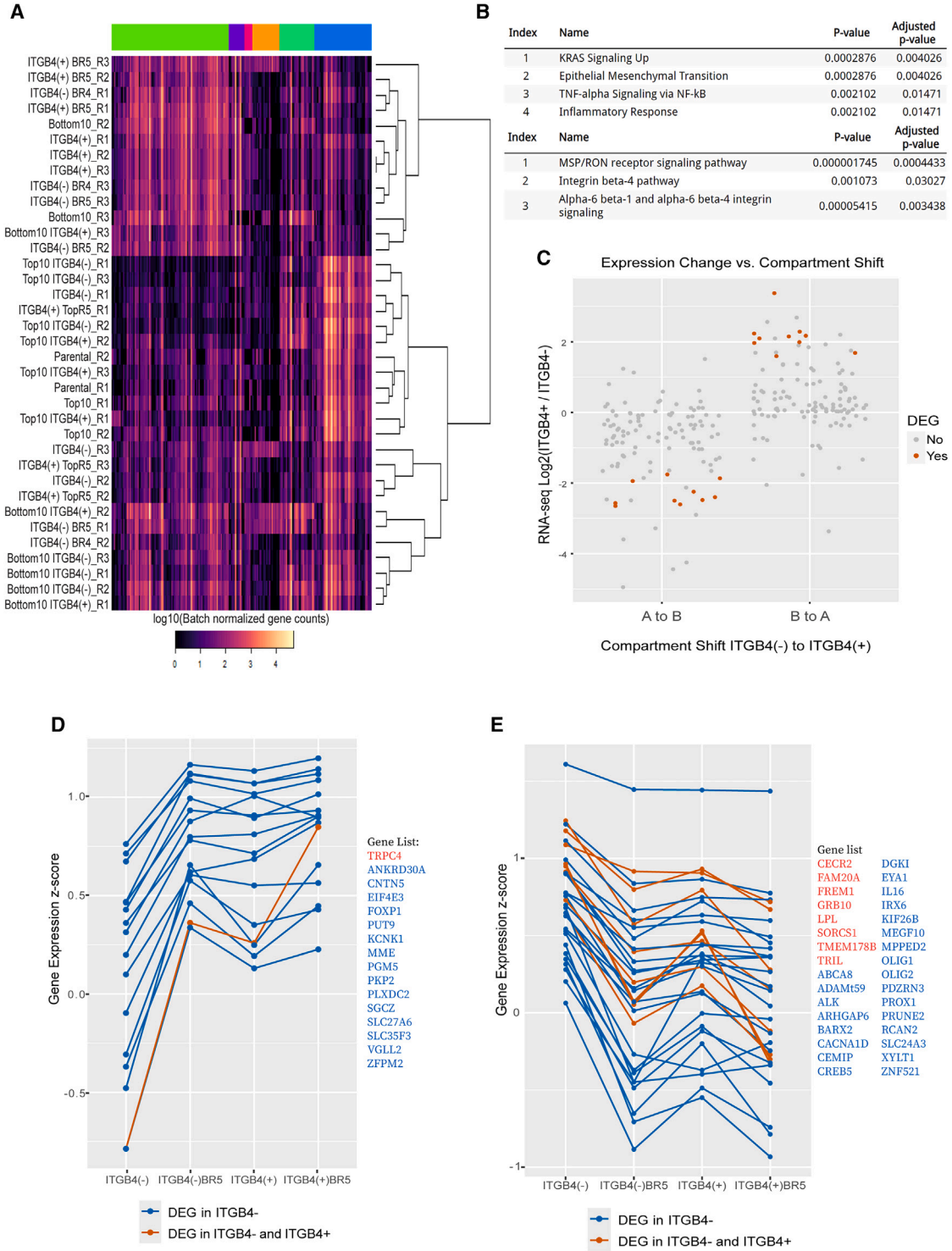

Index	Name	P-value	Adjusted p-value
1	KRAS Signaling Up	0.0002876	0.004026
2	Epithelial Mesenchymal Transition	0.0002876	0.004026
3	TNF-alpha Signaling via NF-kB	0.002102	0.01471
4	Inflammatory Response	0.002102	0.01471

Index	Name	P-value	Adjusted p-value
1	MSP/RON receptor signaling pathway	0.000001745	0.0004433
2	Integrin beta-4 pathway	0.001073	0.03027
3	Alpha-6 beta-1 and alpha-6 beta-4 integrin signaling	0.00005415	0.003438

Figure 7. Gene expression changes partially correlate with compartment shifts following constricted migration

(A) The top 500 most variable genes were used to cluster RNA-seq data across 10 conditions (3 replicates each). Light colored genes are more expressed while dark colored genes are less expressed. Top colorbar shows hierarchical clustering on the genes. The lime cluster represents genes upregulated in migratory cells while the blue cluster represents genes upregulated in the non-migratory cell conditions.

(B) Pathway enrichment analysis of the Lime cluster of genes (upregulated in migratory cells) using EnrichR (MSigDB Hallmark 2020 and NCI-Nature 2016).

(legend continued on next page)

18 is gene poor and peripherally located. This suggests that chromosome gene density and localization may influence susceptibility to constriction-induced compartment switches. Overall, these data suggest that constricted migration can have an effect on 3D genome structure and that there are regions of the genome that are more susceptible to compartment shifts and switches than others.

Gene expression changes partially correlate with compartment shifts following constricted migration

After identifying compartment shifts and switches in our Hi-C analysis, we next asked whether genes in those regions had altered gene expression. We performed RNA-seq on cell populations from a spectrum of ITGB4 and migration conditions and clustered the conditions based on their RNA expression profiles (Figure 7A). Similar to the compartment profiles, migratory cells clustered together and separately from non-migratory cells based on RNA profiles. The analysis found 6 gene clusters that best accounted for the variance with the most notable being the lime cluster, upregulated in migratory cells, and the light blue cluster, upregulated in the non-migratory cluster. EnrichR[35] analysis of the genes within the lime cluster showed us that multiple pathways such as an increase in KRAS signaling and epithelial to mesenchymal transition, as well as the NF-KB inflammatory pathway, were all upregulated in our more migratory populations (Figure 7B). These pathways correlate with an increase in cancer progression and would be expected to be found in more migratory cells. Interestingly, we also found that the ITGB4 pathway was also enriched in the migratory cells, matching nicely with our protein expression flow cytometry data.

Next, we asked whether these gene expression differences among cell populations corresponded to compartment shifts we had observed. We first took the list of genomic regions that switched compartments between ITGB4(−) and ITGB4(+) cell populations and looked at the RNA expression profiles of the genes in these regions in the same cell groups. While only a few of these genes were classified as significantly differently expressed, we observed that the level of RNA expression shifted in the direction expected based on the compartment shift (A to B showing downregulation in ITGB4(+) vs. ITGB4(−) and B to A showing upregulation; Figure 7C). Functional enrichment analysis of the genes in these compartment-switched regions revealed that genes switching to the A compartment in ITGB4(+) cells have been previously annotated as involved in melanoma and skin cancer, cell adhesion, and the development of cell projections, which could be relevant to increase migration (Table S1). Meanwhile, negative regulators of Wnt signaling are shifted to the B compartment in ITGB4(+) cells (Table S1). Moving Wnt signaling inhibitor genes to a repressive environment could in turn increase Wnt signaling, which has been associated with increased cell migration, invasion, and EMT in melanoma.[36–38] Genes with altered compartments in ITGB4(+) vs. (−) cells are also frequently annotated as marked by H3K27me3 in a variety of tissues that have been profiled by the ENCODE project (Table S2). In particular, a large majority of the genes that significantly change expression along with shifting compartment are found to be marked by H3K27me3 in profiled epithelial cell lines.

We next examined genes in the regions that shifted following migration of ITGB4(−) and ITGB4(+) cells. We observed that for both B to A shifts (Figure 7D) and A to B shifts (Figure 7E), genes that change expression move in the same direction as the compartment shifts (compare to Figure 6C and see examples in Figure S4H). Only a subset (~10%) of the genes found in these compartment shifting regions were differentially expressed, and of the entire cohort of differentially expressed genes, only a small fraction were found to be within our shifted/switched genomic regions. This suggests that compartment switching is not only for the purpose of facilitating gene regulation, but could also play a role in the physical state of the cell. However, those genes that did change were concordant with the direction of the compartment shift. Certain genes that shifted compartment with constricted migration showed relevant functional enrichments, including regulation of endothelial cell migration, cell-cell adhesion, actin-based cell projection, and sensory perception of mechanical stimulus (Table S3). Certain interesting candidate players in enhanced migration were identified among the genes that were both differentially expressed and shifted compartments with constricted migration. For example, TRPC4 was shifted toward the A compartment and upregulated after constricted migration in both ITGB4(−) and ITGB4(+) cells (Figure 7D). TRPC4 is a calcium channel that is a part of a mechanosensitive family of channels,[39] is physically linked to the actin cytoskeleton,[40] and has been previously associated with enhanced migration in medulloblastoma.[41] Genes like this that are specifically induced by constricted migration could link mechanical force to migratory potential. However, while compartment shifting that results from constriction may help activate or repress certain key migration genes, gene regulation is likely not the only function of or explanation for the compartment shifts. As with ITGB4(+) compartment shifts, migration-specific compartment shifts tended to occur in genomic regions that have been annotated to be marked with H3K27me3. Annotation with H3K27me3 is particularly enriched for genes that are both differentially regulated and shift compartments (Table S4).

DISCUSSION

Many factors are involved in determining whether cancer cells will metastasize and what their phenotype will be once they reach a distant site. Here, we focused on one part of this complex process: the ability of A375 melanoma cells to migrate

(C) Gene expression changes from ITGB4(−) to (+) cells for the genes in ITGB4(−) to (+) compartment changes. Significantly differentially expressed genes are shown in orange, others gray.
(D) Gene expression *Z* score across ITGB4 conditions for genes in the 250 kb bins with positive compartment shift slopes (Figure 7A). Blue = differentially expressed in ITGB4(−) vs. ITGB4(−)BR5. Orange = significantly differentially expressed in both ITGB4(+) and ITGB4(−) cells after 5 rounds of migration. The gene list is provided to the right.
(E) Gene expression *Z* score across ITGB4 conditions for genes in the 250 kb bins with negative compartment shift slopes (Figure 7A). Colors as in (D).

through constrictions smaller than their nucleus. Previous work had identified 3D genome structure changes and gene expression changes in melanoma cells that had migrated through 10 rounds of constriction and gained a highly invasive phenotype,[10] but it was unclear whether these differences arose from a pre-existing subpopulation selected by the rounds of migration or whether they were induced during the process of constriction. Here, our results have begun to disentangle this conundrum. We identified a cell surface protein, ITGB4, that was highly expressed across all our highly migratory sequentially constricted cells, and we found that ITGB4 was already expressed on a subpopulation of cells before migration. We found that sorting out high ITGB4-expressing cells from the parental A375 population yielded a subgroup of cells that were already as migratory as the cells that had passed through 10 rounds of constriction (Bottom10). This result, by itself, could mean that the "changes" we saw in sequentially constricted cells were simply the result of isolating this already highly migratory ITGB4 expressing population. However, further investigation revealed that there are key ways that sequentially constricted Bottom10 cells are different from this initial migratory ITGB4(+) subpopulation. Examining cellular elongation, behavior when embedded in 3D collagen matrices, and ability to migrate through even smaller pores, it became clear that this initial ITGB4(+) population is an intermediate between the non-migratory cells in the initial population and the highly invasive cells after sequential passage through constrictions. Therefore, detailed analysis and further migration of this ITGB4(+) subpopulation provided us a window into what genome architecture differences pre-exist and which are induced by sequential constriction.

ITGB4 expression by itself is not sufficient to explain why this initial subpopulation is more proficient at constricted migration, since knocking down ITGB4 resulted in only modest decreases in migration. Instead, this subpopulation contains 3D genome architecture and gene expression differences throughout the genome that could play a role in defining an initially increased migration ability. Indeed, both by genome compartment signatures and gene expression signatures, ITGB4(+) cells clustered with highly migratory cells, and genes defining these differential signatures were involved in metastasis and migration-relevant processes such as epithelial-mesenchymal transition. Whether we started from the entire parental A375 population, or a population grown from a single cell clone, we found that ITGB4(+) cells showed consistent regions of the genome with altered compartmentalization as compared to ITGB4(−) cells.

As with their cellular appearance and behavior, the genome structure state of ITGB4(+) cells is an intermediate between the parental population and the Bottom10 cells. Further changes to the 3D genome occur in these cells only after constricted migration. Our finding that many genome structure changes are shared whether initially ITGB4(+) or ITGB4(−) cells are subjected to several rounds of constricted migration suggests that there are indeed certain genomic regions that are particularly susceptible to change with passage through constrictions.

Interestingly, these further changes that happen to cells after constricted migration not only make the cells better at migrating through even smaller constrictions, but also remove any dependence on ITGB4 for migration. We propose that, in this way, ITGB4 expression is conceptually similar to training wheels on a bicycle. Initially, for an inexperienced rider, training wheels provide important assistance, and removing them would increase the likelihood that a rider would fall, just as removing ITGB4 from a cell that is not yet "experienced" with constricted migration results in somewhat decreased migratory ability. But, once a rider has undergone further training and experience, removing the training wheels would make little difference, just as removing ITGB4 from Bottom10 cells no longer influences migration rates.

Our results also reveal that the final state of cells after sequential constriction is not simply a matter of selecting cells that already express ITGB4 and then further remodeling them through the process of constriction. Within our populations grown from individual cell clones, which have reduced heterogeneity, we have examples where almost no cells expressed ITGB4 initially, but still, after 10 rounds of constriction, ITGB4 became highly expressed. By carefully tracking ITGB4 surface protein levels before and after each round of migration, we found that signatures of selection were indeed present: more ITGB4-expressing cells were found immediately after passage through pores than before. However, substantial increases in migration and ITGB4 expression required multiple rounds of constriction. Further, there were also cases where ITGB4 expression was increased during cell growth between rounds of migration, suggesting that passage through the constriction activates processes which can continue to change the cell phenotype even after that acute stress is over. This experiment also clarified that it is truly the constriction, not other factors in the migration process, that results in ITGB4 increase: cells passing through wide 12 μm pores were exposed to the same fibronectin and growth media conditions, but did not show increases in ITGB4 expression over time.

Overall, our study reveals that 3D genome structure differences may be important both for encoding an initial highly migratory cell identity as well as for stabilizing the further alterations in cell phenotype that occur after constricted migration. This conclusion is in line with other work in the field that emphasizes the importance of genome spatial compartmentalization in defining cell fate and cell type.[19] Further work will be needed to identify what triggers and pathways are activating increases in ITGB4 and causing other changes to the 3D genome structure. With the sets of regions identified here, future work can investigate what properties make a genomic region a hotspot susceptible to compartment change after constricted migration. One notable feature among the regions we identified is that gene poor, peripherally located chromosomes experienced more changes than gene rich internal chromosomes. Coinciding with this, it is important to note that while gene expression levels correlated with the compartment alterations we observed, only a small subset of genes experienced changes in expression. This suggests, as described previously,[42,43] that the migration-favoring 3D genome alterations can also be important to nucleus physical properties rather than only gene regulation.

We expect that the changes we observe here relate to the physical microenvironment-induced alterations in chromatin modifying enzymes that have been shown in other contexts.[11,12,22] Indeed, initial analysis suggests that one common feature between the genomic regions that change compartment

with constriction is their tendency to be marked with H3K27me3 (according to annotations in EnrichR). This suggests that the changes in this mark that can be induced by passage through constrictions[22] could result in the long-term compartment alterations we observe here.

From a therapeutic perspective, analysis of available data in cancer patients has previously shown that ITGB4 expression is correlated with patient prognosis and survival across numerous types of cancer.[29] ITGB4 shows significantly increased transcription in tumors in 23 of the 33 cancer types with available TCGA data. Increased expression of ITGB4 is associated with poor prognosis (shorter overall survival or disease-free survival) for the majority of cancer types (20 of the 33). Skin cancer patients showed the highest frequencies of mutations in ITGB4 of all the cancer types examined. However, not enough data exists to evaluate the connection between ITGB4 expression and metastasis in melanoma patients. Only a few patient samples available in the cBioPortal (v.6.0.23)[44,45] have RNA-seq data collected along with metastatic status, and none have ITGB4 protein expression measured. Our results suggest that future study is warranted to quantify ITGB4 expression status in metastatic melanoma in patients. Beyond a single protein, however, our results indicate that there are likely to be RNA and 3D genome signatures within subpopulations of cells in a tumor that indicate a cell's initial propensity to undergo migration. Such invasive gene expression signatures have previously been discussed,[46,47] but our study clarifies pre-existing 3D genome signatures and how these may further change during the process of cell migration. Our results also show that a whole suite of cellular and genomic changes accompany ITGB4 status, and knocking down ITGB4 only modestly reduces migration. Thus, our results also caution against using a single factor like ITGB4 as a prognostic marker or therapeutic target.

Limitations of the study

When analyzing specific genomic regions that alter their gene expression or structure during a process like constricted cell migration, we are always faced with a tradeoff between the depth of information we can obtain, the precision of genomic localization, and the ability to track a cell in real time. In this study, we have used sub-population sorting to examine differences within a heterogeneous cell population. However, even within a population grown from a single cell clone or sorted based on certain characteristics, we know that there is still inherent heterogeneity and cell to cell variability that is not captured in our bulk Hi-C and RNA-seq analyses. Further, even when we do track individual cell properties such as ITGB4 surface protein expression, aspect ratio, or behavior in 3D collagen matrices, we are limited to cells at certain time points (before migration, after each round of migration) rather than tracking changes in an individual cell over time. Finally, we are examining a single melanoma cell line. Our past work suggests that some of the 3D genome structure alterations we observe are shared even among different cancer types,[10] but the specific signatures of migration ability may differ for cells from different patients or different tumor starting points.

RESOURCE AVAILABILITY

Lead contact

Requests for further information and resources should be directed to and will be fulfilled by the lead contact, Rachel Patton McCord (rmccord@utk.edu).

Materials availability

All unique/stable reagents generated in this study are available from the lead contact with a completed materials transfer agreement.

Data and code availability

- Raw and processed Hi-C and RNA-seq data files are available at GEO accession number GSE275397 and are publicly available as of the date of publication.
- All numeric and tabular data associated with figures, as well as unprocessed image and flow cytometry data files have been deposited at Mendeley Data: Playter, Christopher et al. (2025), "ITGB4 in Human A375 Melanoma Constricted Migration – Imaging and Flow Cytometry Datasets", Mendeley Data, V1, https://doi.org/10.17632/cfyrmwsf8y.1 and are publicly available as of the date of publication.
- This paper does not report original code.
- Any additional information required to reanalyze the data reported in this paper is available from the lead contact upon request.

ACKNOWLEDGMENTS

We thank all members of the McCord lab for helpful discussion and feedback. We thank Dibyayan Maity and Tehya Daniels for their help with early troubleshooting experiments. We acknowledge the UTK Advanced Microscopy and Imaging Center and Genomics Core for assistance with imaging and sequencing and Trevor Hancock for assistance with flow cytometry. We thank Chandler Ross for assistance with image analysis. This work was supported by the National Institutes of Health [NIGMS grant R35GM133557 to R.P.M].

AUTHOR CONTRIBUTIONS

C.P. and R.P.M. designed the study. C.P., R.G., T.H.O., S.J.B., and A.S. performed experiments. R.P.M., J.H.G. and A.R.G. performed bioinformatic analyses. C.P. and R.P.M. wrote the paper with contributions from all authors.

DECLARATION OF INTERESTS

Rachel Patton McCord is a member of the Cell Press Statistical Advisory Board.

STAR★METHODS

Detailed methods are provided in the online version of this paper and include the following:

- KEY RESOURCES TABLE
- EXPERIMENTAL MODEL AND STUDY PARTICIPANT DETAILS
  - A375 cell culture
- METHOD DETAILS
  - Transwell migration assays
  - Flow cytometry and fluorescence activated cell sorting
  - Flow cytometry and FACS analysis
  - Scratch assay
  - 3D collagen matrix
  - Confluence and media depletion tests
  - ITGB4 RNAi
  - Hi-C experiments
  - Hi-C data analysis
  - RNA-seq experiments
  - RNA-seq analysis
- QUANTIFICATION AND STATISTICAL ANALYSIS

SUPPLEMENTAL INFORMATION

Supplemental information can be found online at https://doi.org/10.1016/j.isci.2025.112346.

Received: August 22, 2024
Revised: January 22, 2025
Accepted: March 31, 2025
Published: April 3, 2025

REFERENCES

1. Winnard, P.T., Jr., Pathak, A.P., Dhara, S., Cho, S.Y., Raman, V., and Pomper, M.G. (2008). Molecular imaging of metastatic potential. J. Nucl. Med. *49*, 96S–112S. https://doi.org/10.2967/jnumed.107.045948.
2. Calbo, J., van Montfort, E., Proost, N., van Drunen, E., Beverloo, H.B., Meuwissen, R., and Berns, A. (2011). A Functional Role for Tumor Cell Heterogeneity in a Mouse Model of Small Cell Lung Cancer. Cancer Cell *19*, 244–256. https://doi.org/10.1016/j.ccr.2010.12.021.
3. Lambert, A.W., Pattabiraman, D.R., and Weinberg, R.A. (2017). Emerging Biological Principles of Metastasis. Cell *168*, 670–691. https://doi.org/10.1016/j.cell.2016.11.037.
4. Omar, A.M., and Abdellatef, A.A. (2024). Differential Analyses of Leader and Follower Cancer Cells. Future Perspect. Med. Pharm. Environ. Biotechnol. *1*, 12–16. https://doi.org/10.21608/fpmpeb.2024.305982.1010.
5. Salcido, C.D., Larochelle, A., Taylor, B.J., Dunbar, C.E., and Varticovski, L. (2010). Molecular characterisation of side population cells with cancer stem cell-like characteristics in small-cell lung cancer. Br. J. Cancer *102*, 1636–1644. https://doi.org/10.1038/sj.bjc.6605668.
6. Perkins, R.S., Murray, G., Suthon, S., Davis, L., Perkins, N.B., 3rd, Fletcher, L., Bozzi, A., Schreiber, S.L., Lin, J., Laxton, S., et al. (2024). WNT5B drives osteosarcoma stemness, chemoresistance and metastasis. Clin. Transl. Med. *14*, e1670. https://doi.org/10.1002/ctm2.1670.
7. Groves, S.M., Ildefonso, G.V., McAtee, C.O., Ozawa, P.M.M., Ireland, A.S., Stauffer, P.E., Wasdin, P.T., Huang, X., Qiao, Y., Lim, J.S., et al. (2022). Archetype tasks link intratumoral heterogeneity to plasticity and cancer hallmarks in small cell lung cancer. Cell Syst. *13*, 690–710.e17. https://doi.org/10.1016/j.cels.2022.07.006.
8. Gambardella, G., Viscido, G., Tumaini, B., Isacchi, A., Bosotti, R., and di Bernardo, D. (2022). A single-cell analysis of breast cancer cell lines to study tumour heterogeneity and drug response. Nat. Commun. *13*, 1714. https://doi.org/10.1038/s41467-022-29358-6.
9. Kozlowski, J.M., Hart, I.R., Fidler, I.J., and Hanna, N. (1984). A human melanoma line heterogeneous with respect to metastatic capacity in athymic nude mice. J. Natl. Cancer Inst. *72*, 913–917.
10. Golloshi, R., Playter, C., Freeman, T.F., Das, P., Raines, T.I., Garretson, J.H., Thurston, D., and McCord, R.P. (2022). Constricted migration is associated with stable 3D genome structure differences in cancer cells. EMBO Rep. *23*, e52149. https://doi.org/10.15252/embr.202052149.
11. Song, M., Jang, Y., Kim, S.-J., and Park, Y. (2022). Cyclic Stretching Induces Maturation of Human-Induced Pluripotent Stem Cell-Derived Cardiomyocytes through Nuclear-Mechanotransduction. Tissue Eng. Regen. Med. *19*, 781–792. https://doi.org/10.1007/s13770-021-00427-z.
12. Heo, S.-J., Thakur, S., Chen, X., Loebel, C., Xia, B., McBeath, R., Burdick, J.A., Shenoy, V.B., Mauck, R.L., and Lakadamyali, M. (2023). Aberrant chromatin reorganization in cells from diseased fibrous connective tissue in response to altered chemomechanical cues. Nat. Biomed. Eng. *7*, 177–191. https://doi.org/10.1038/s41551-022-00910-5.
13. Smith, L.R., Cho, S., and Discher, D.E. (2018). Stem Cell Differentiation is Regulated by Extracellular Matrix Mechanics. Physiology *33*, 16–25. https://doi.org/10.1152/physiol.00026.2017.
14. Barutcu, A.R., Lajoie, B.R., McCord, R.P., Tye, C.E., Hong, D., Messier, T.L., Browne, G., van Wijnen, A.J., Lian, J.B., Stein, J.L., et al. (2015). Chromatin interaction analysis reveals changes in small chromosome and telomere clustering between epithelial and breast cancer cells. Genome Biol. *16*, 214. https://doi.org/10.1186/s13059-015-0768-0.
15. Harewood, L., Kishore, K., Eldridge, M.D., Wingett, S., Pearson, D., Schoenfelder, S., Collins, V.P., and Fraser, P. (2017). Hi-C as a tool for precise detection and characterisation of chromosomal rearrangements and copy number variation in human tumours. Genome Biol. *18*, 125. https://doi.org/10.1186/s13059-017-1253-8.
16. San Martin, R., Das, P., Dos Reis Marques, R., Xu, Y., Roberts, J.M., Sanders, J.T., Golloshi, R., and McCord, R.P. (2022). Chromosome compartmentalization alterations in prostate cancer cell lines model disease progression. J. Cell Biol. *221*, e202104108. https://doi.org/10.1083/jcb.202104108.
17. Pang, Q.Y., Tan, T.Z., Sundararajan, V., Chiu, Y.-C., Chee, E.Y.W., Chung, V.Y., Choolani, M.A., and Huang, R.Y.-J. (2022). 3D genome organization in the epithelial-mesenchymal transition spectrum. Genome Biol. *23*, 121. https://doi.org/10.1186/s13059-022-02687-x.
18. Achinger-Kawecka, J., Valdes-Mora, F., Luu, P.-L., Giles, K.A., Caldon, C.E., Qu, W., Nair, S., Soto, S., Locke, W.J., Yeo-Teh, N.S., et al. (2020). Epigenetic reprogramming at estrogen-receptor binding sites alters 3D chromatin landscape in endocrine-resistant breast cancer. Nat. Commun. *11*, 320. https://doi.org/10.1038/s41467-019-14098-x.
19. Li, H., Playter, C., Das, P., and McCord, R.P. (2024). Chromosome compartmentalization: causes, changes, consequences, and conundrums. Trends Cell Biol. *34*, 707–727. https://doi.org/10.1016/j.tcb.2024.01.009.
20. Vilarrasa-Blasi, R., Soler-Vila, P., Verdaguer-Dot, N., Russiñol, N., Di Stefano, M., Chapaprieta, V., Clot, G., Farabella, I., Cuscó, P., Kulis, M., et al. (2021). Dynamics of genome architecture and chromatin function during human B cell differentiation and neoplastic transformation. Nat. Commun. *12*, 651. https://doi.org/10.1038/s41467-020-20849-y.
21. Owen, J.A., Osmanović, D., and Mirny, L. (2023). Design principles of 3D epigenetic memory systems. Science *382*, eadg3053. https://doi.org/10.1126/science.adg3053.
22. Hsia, C.R., McAllister, J., Hasan, O., Judd, J., Lee, S., Agrawal, R., Chang, C.Y., Soloway, P., and Lammerding, J. (2022). Confined migration induces heterochromatin formation and alters chromatin accessibility. iScience *25*, 104978. https://doi.org/10.1016/j.isci.2022.104978.
23. Nordick, B., Yu, P.Y., Liao, G., and Hong, T. (2022). Nonmodular oscillator and switch based on RNA decay drive regeneration of multimodal gene expression. Nucleic Acids Res. *50*, 3693–3708. https://doi.org/10.1093/nar/gkac217.
24. Stewart, R.L., and O'Connor, K.L. (2015). Clinical significance of the integrin alpha6beta4 in human malignancies. Lab. Invest. *95*, 976–986. https://doi.org/10.1038/labinvest.2015.82.
25. Meng, X., Liu, P., Wu, Y., Liu, X., Huang, Y., Yu, B., Han, J., Jin, H., and Tan, X. (2020). Integrin beta 4 (ITGB4) and its tyrosine-1510 phosphorylation promote pancreatic tumorigenesis and regulate the MEK1-ERK1/2 signaling pathway. Bosn. J. Basic Med. Sci. *20*, 106–116. https://doi.org/10.17305/bjbms.2019.4255.
26. Wilkinson, E.J., Woodworth, A.M., Parker, M., Phillips, J.L., Malley, R.C., Dickinson, J.L., and Holloway, A.F. (2020). Epigenetic regulation of the ITGB4 gene in prostate cancer. Exp. Cell Res. *392*, 112055. https://doi.org/10.1016/j.yexcr.2020.112055.
27. Li, M., Jiang, X., Wang, G., Zhai, C., Liu, Y., Li, H., Zhang, Y., Yu, W., and Zhao, Z. (2019). ITGB4 is a novel prognostic factor in colon cancer. J. Cancer *10*, 5223–5233. https://doi.org/10.7150/jca.29269.
28. Li, X.L., Liu, L., Li, D.D., He, Y.P., Guo, L.H., Sun, L.P., Liu, L.N., Xu, H.X., and Zhang, X.P. (2017). Integrin beta4 promotes cell invasion and epithelial-mesenchymal transition through the modulation of Slug expression in hepatocellular carcinoma. Sci. Rep. *7*, 40464. https://doi.org/10.1038/srep40464.

29. Huang, W., Fan, L., Tang, Y., Chi, Y., and Li, J. (2021). A Pan-Cancer Analysis of the Oncogenic Role of Integrin Beta4 (ITGB4) in Human Tumors. Int. J. Gen. Med. *14*, 9629–9645. https://doi.org/10.2147/IJGM.S341076.

30. Li, G.S., Huang, Z.G., He, R.Q., Zhang, W., Tang, Y.X., Liu, Z.S., Gan, X.Y., Tang, D., Li, D.M., Tang, Y.L., et al. (2024). ITGB4 Serves as an Identification and Prognosis Marker Associated with Immune Infiltration in Small Cell Lung Carcinoma. Mol. Biotechnol. *66*, 2956–2971. https://doi.org/10.1007/s12033-023-00912-x.

31. Nurzat, Y., Su, W., Min, P., Li, K., Xu, H., and Zhang, Y. (2021). Identification of Therapeutic Targets and Prognostic Biomarkers Among Integrin Subunits in the Skin Cutaneous Melanoma Microenvironment. Front. Oncol. *11*, 751875. https://doi.org/10.3389/fonc.2021.751875.

32. Bourget, J.-M., Morcos, M., Zaniolo, K., Gü¦rin, S.L., and Proulx, S.p. (2015). Influence of Cell Confluency on the Expression of the ¦Á4 Integrin Subunit of Retinal Pigment Epithelial Cells. Adv. Biol. Chem. *10*, 55168. https://doi.org/10.4236/abc.2015.52007.

33. Muranen, T., Iwanicki, M.P., Curry, N.L., Hwang, J., DuBois, C.D., Coloff, J.L., Hitchcock, D.S., Clish, C.B., Brugge, J.S., and Kalaany, N.Y. (2017). Starved epithelial cells uptake extracellular matrix for survival. Nat. Commun. *8*, 13989. https://doi.org/10.1038/ncomms13989.

34. Wolfe, D., Dudek, S., Ritchie, M.D., and Pendergrass, S.A. (2013). Visualizing genomic information across chromosomes with PhenoGram. BioData Min. *6*, 18. https://doi.org/10.1186/1756-0381-6-18.

35. Xie, Z., Bailey, A., Kuleshov, M.V., Clarke, D.J.B., Evangelista, J.E., Jenkins, S.L., Lachmann, A., Wojciechowicz, M.L., Kropiwnicki, E., Jagodnik, K.M., et al. (2021). Gene Set Knowledge Discovery with Enrichr. Curr. Protoc. *1*, e90. https://doi.org/10.1002/cpz1.90.

36. Sinnberg, T., Levesque, M.P., Krochmann, J., Cheng, P.F., Ikenberg, K., Meraz-Torres, F., Niessner, H., Garbe, C., and Busch, C. (2018). Wnt-signaling enhances neural crest migration of melanoma cells and induces an invasive phenotype. Mol. Cancer *17*, 59. https://doi.org/10.1186/s12943-018-0773-5.

37. Deng, W., Fernandez, A., McLaughlin, S.L., and Klinke, D.J., II. (2019). WNT1-inducible signaling pathway protein 1 (WISP1/CCN4) stimulates melanoma invasion and metastasis by promoting the epithelial–mesenchymal transition. J. Biol. Chem. *294*, 5261–5280. https://doi.org/10.1074/jbc.RA118.006122.

38. Webster, M.R., Kugel, C.H., and Weeraratna, A.T. (2015). The Wnts of change: How Wnts regulate phenotype switching in melanoma. Biochim. Biophys. Acta *1856*, 244–251. https://doi.org/10.1016/j.bbcan.2015.10.002.

39. Canales Coutiño, B., and Mayor, R. (2021). Mechanosensitive ion channels in cell migration. Cells Dev. *166*, 203683. https://doi.org/10.1016/j.cdev.2021.203683.

40. Canales, J., Morales, D., Blanco, C., Rivas, J., Díaz, N., Angelopoulos, I., and Cerda, O. (2019). A TR(i)P to Cell Migration: New Roles of TRP Channels in Mechanotransduction and Cancer. Front. Physiol. *10*, 757. https://doi.org/10.3389/fphys.2019.00757.

41. Wei, W.-C., Huang, W.-C., Lin, Y.-P., Becker, E.B.E., Ansorge, O., Flockerzi, V., Conti, D., Cenacchi, G., and Glitsch, M.D. (2017). Functional expression of calcium-permeable canonical transient receptor potential 4-containing channels promotes migration of medulloblastoma cells. J. Physiol. *595*, 5525–5544. https://doi.org/10.1113/JP274659.

42. Heo, S.-J., Song, K.H., Thakur, S., Miller, L.M., Cao, X., Peredo, A.P., Seiber, B.N., Qu, F., Driscoll, T.P., Shenoy, V.B., et al. (2020). Nuclear softening expedites interstitial cell migration in fibrous networks and dense connective tissues. Sci. Adv. *6*, eaax5083. https://doi.org/10.1126/sciadv.aax5083.

43. Bustin, M., and Misteli, T. (2016). Nongenetic functions of the genome. Science *352*, aad6933. https://doi.org/10.1126/science.aad6933.

44. Cerami, E., Gao, J., Dogrusoz, U., Gross, B.E., Sumer, S.O., Aksoy, B.A., Jacobsen, A., Byrne, C.J., Heuer, M.L., Larsson, E., et al. (2012). The cBio Cancer Genomics Portal: An Open Platform for Exploring Multidimensional Cancer Genomics Data. Cancer Discov. *2*, 401–404. https://doi.org/10.1158/2159-8290.Cd-12-0095.

45. Gao, J., Aksoy, B.A., Dogrusoz, U., Dresdner, G., Gross, B., Sumer, S.O., Sun, Y., Jacobsen, A., Sinha, R., Larsson, E., et al. (2013). Integrative analysis of complex cancer genomics and clinical profiles using the cBioPortal. Sci. Signal. *6*, pl1. https://doi.org/10.1126/scisignal.2004088.

46. Jeffs, A.R., Glover, A.C., Slobbe, L.J., Wang, L., He, S., Hazlett, J.A., Awasthi, A., Woolley, A.G., Marshall, E.S., Joseph, W.R., et al. (2009). A gene expression signature of invasive potential in metastatic melanoma cells. PLoS One *4*, e8461. https://doi.org/10.1371/journal.pone.0008461.

47. Rapanotti, M.C., Campione, E., Suarez Viguria, T.M., Spallone, G., Costanza, G., Rossi, P., Orlandi, A., Valenti, P., Bernardini, S., and Bianchi, L. (2020). Stem–Mesenchymal Signature Cell Genes Detected in Heterogeneous Circulating Melanoma Cells Correlate With Disease Stage in Melanoma Patients. Front. Mol. Biosci. *7*, 92. https://doi.org/10.3389/fmolb.2020.00092.

48. Denais, C.M., Gilbert, R.M., Isermann, P., McGregor, A.L., te Lindert, M., Weigelin, B., Davidson, P.M., Friedl, P., Wolf, K., and Lammerding, J. (2016). Nuclear envelope rupture and repair during cancer cell migration. Science *352*, 353–358. https://doi.org/10.1126/science.aad7297.

49. Langmead, B., and Salzberg, S.L. (2012). Fast gapped-read alignment with Bowtie 2. Nat. Methods *9*, 357–359. https://doi.org/10.1038/nmeth.1923.

50. Dobin, A., Davis, C.A., Schlesinger, F., Drenkow, J., Zaleski, C., Jha, S., Batut, P., Chaisson, M., and Gingeras, T.R. (2013). STAR: ultrafast universal RNA-seq aligner. Bioinformatics *29*, 15–21. https://doi.org/10.1093/bioinformatics/bts635.

51. Zhang, Y., Liu, T., Meyer, C.A., Eeckhoute, J., Johnson, D.S., Bernstein, B.E., Nusbaum, C., Myers, R.M., Brown, M., Li, W., and Liu, X.S. (2008). Model-based analysis of ChIP-Seq (MACS). Genome Biol. *9*, R137. https://doi.org/10.1186/gb-2008-9-9-r137.

52. Anders, S., Pyl, P.T., and Huber, W. (2015). HTSeq–a Python framework to work with high-throughput sequencing data. Bioinformatics *31*, 166–169. https://doi.org/10.1093/bioinformatics/btu638.

53. Love, M.I., Huber, W., and Anders, S. (2014). Moderated estimation of fold change and dispersion for RNA-seq data with DESeq2. Genome Biol. *15*, 550. https://doi.org/10.1186/s13059-014-0550-8.

54. Quinlan, A.R., and Hall, I.M. (2010). BEDTools: a flexible suite of utilities for comparing genomic features. Bioinformatics *26*, 841–842. https://doi.org/10.1093/bioinformatics/btq033.

STAR★METHODS

KEY RESOURCES TABLE

REAGENT or RESOURCE	SOURCE	IDENTIFIER
Antibodies		
ITGB4-FITC	Abcam	Cat# ab22486; RRID:AB_447091
Chemicals, peptides, and recombinant proteins		
DMEM	Corning	10-013-CV
FBS	Corning	35-010-CV
Pen-Strep	Gibco	14140-122
L-Glutamine	Gibco	25030-081
Trypsin	Corning	25053CI
Collagen	Corning	354236
Protease inhibitors/EDTA	GenDepot	50-101-5485
Phosphatase inhibitors	GenDepot	50-101-5488
Fibronectin	Corning	354008
Critical commercial assays		
Arima-HiC+ Kit	Arima	A510008
RNA easy Kit	Qiagen	74134
Ultra II RNA library prep kit	New England Biolabs	E7770G
Multiplex Oligos for Illumina	New England Biolabs	E7335G
Human ITGB4 siRNA SMARTpool	Dharmacon	L-008011-00-0005
Non-targeting Pool	Dharmacon	D-001810-10-05
siRNA Buffer	Dharmacon	B-002000-UB-100
DharmaFECT1 Transfection Agent	Dharmacon	T-2001-01
Deposited data		
Hi-C, RNA-Seq from A375 cell lines	This study	GEO:GSE275397
Tabular data, raw images, flow cytometry files	This study	Mendeley Data: https://doi.org/10.17632/cfyrmwsf8y.1
Experimental models: Cell lines		
A375	ATCC	CRL-1619
Software and algorithms		
Bowtie2	Langmead and Salzberg[49]	http://bowtie-bio.sourceforge.net/bowtie2/index.shtml
C-World		https://github.com/dekkerlab/cworld-dekker
STAR	Dobin et al.[50]	https://github.com/alexdobin/STAR
MACS2	Zhang et al.[51]	https://github.com/taoliu/MACS
HTSeq	Anders et al.[52]	https://htseq.readthedocs.io/
DESeq2	Love et al.[53]	https://bioconductor.org/packages/release/bioc/html/DESEQ2.html
Bedtools	Quinlan et al.[54]	http://bedtools.readthedocs.io/en/latest/
GraphPad Prism (statistical tests)		https://www.graphpad.com/
Other		
Transwell Filters (12μm)	VWR	10769-224
Transwell Filters (5μm)	VWR	10769-236

EXPERIMENTAL MODEL AND STUDY PARTICIPANT DETAILS

A375 cell culture

A375 human melanoma cells (female, XX) were obtained from ATCC (CRL-1619). Cells were verified to be negative for mycoplasma and were grown using complete DMEM medium (Corning-10-013-CV; 10% FBS, 1% Pen-Strep, 1% L-Glutamine) at 37°C supplied with 5% CO_2. Cell line authentication was verified by observing cell line-specific translocations in Hi-C results.

METHOD DETAILS

Transwell migration assays

Transwell filters with 5μm pores (VWR-10769-236) 12μm pores (VWR-10769-224), and 3 μm pores (Corning-353096) were used. Briefly, the bottom of each filter was coated with 40μl of 10 μg/ml fibronectin for ~30 min. 24-well plates were prepared for Transwell migration assay by adding 500 μl of 1× DMEM (Corning) with full supplements per well. A375 cells were detached from culture dishes at 80–90% confluency and aliquoted to 100,000 cells per 100μl of unsupplemented 1×DMEM. Each Transwell was placed into its corresponding well of the 24-well plates, and 100μl of the cell suspension was added to the top of each filter. Cells were incubated at 37°C, 5% CO_2 and allowed to migrate for 24hr.

After the 24hr incubation, migration efficiency was quantified as follows; first, freely floating cells were removed from the top of the filter (unmigrated cells) and from the well beneath the filter (migrated cells) and placed in two separate tubes. Then, 400μl of trypsin was added into the bottom chamber of the 24-well plates, and 200μl of trypsin was added into the top chamber to detach any remaining attached cells. Recovered cells after trypsinization were added to the unmigrated or migrated tubes, accordingly. Cells were spun down (1,000 rpm, 5 min) and resuspended in 100uL of DMEM. 15ul from each tube was collected and counted (using trypan blue) on a hemacytometer to calculate % migration such as: #bottom/(#top+#bottom).

For sequential rounds of migration, the migrated cells were seeded into a new well of a 24-well plate to expand. When cells reached 80–90% confluency, another Transwell migration was performed. Only the bottom cells were collected and continued to be used for sequential rounds of migration.

Flow cytometry and fluorescence activated cell sorting

All cytometry and FACS experiments followed the same protocol for ITGB4 staining. Cells were harvested using trypsin (T25, 6-well, 24-well) and spun at 1000rpm for 5 minutes. Supernatant was removed and cells were resuspended in 400uL of PBS containing 10% FBS and 1.25ug of Abcam FITC Anti-ITGB4 (ab22486). Cells were then incubated on ice for 30 minutes with slight agitation every 10 minutes (flicking) to ensure antibody distribution. Cells were then diluted with 350uL of PBS containing 10% FBS and mixed by pipetting before being spun at 1000rpm for 5 minutes. Supernatant was removed and cells were washed 2 more times with 400uL of PBS containing 10% FBS to ensure excess antibody was washed away. Unfixed cells were used for FACS, but for flow cytometry quantification, cells were then fixed by adding 500uL of 1% formaldehyde and incubated at RT for 10 minutes. Cells then were washed 2 times with 400uL of PBS containing 10% FBS. Finally, cells were suspended in 500uL of PBS containing 10% FBS and run on a flow cytometer.

Flow cytometry and FACS analysis

For FACS experiments, cells were sorted by either a FACS Aria cell sorter (One Hi-C replicate for ITGB4(+) and ITGB4(-) cells, and some initial 5 μm migration experiments) or a Sony MA900 cell sorter (A second Hi-C replicate for ITGB4(+) and (-) cells, Clone 3 (+) and (-) cells and all other experiments). To determine the cutoff for ITGB4 expression, an Unstained cell population was used as a negative control. These cells followed the same staining protocol described above but did not include 1.25ug of the ITGB4 antibody. For the FACS Aria, once the cells were gated for the live population and doublets were removed, anything that expressed ITGB4 (FIT-C) above the Unstained condition was sorted into a (+) tube, while everything else was sorted into a (-) tube. To get a more stringent cutoff for ITGB4(+) and ITGB4(-), we re-sorted using the Sony 6000 sorter and after gating for live cells and removing doublets we again used an Unstained population of cells to get a cutoff, but then set 2 thresholds, one above and one below the Unstained cutoff to create 3 populations. The highly ITGB4 expressing cells were sorted into the (+) tubes, the very little to no ITGB4 expressing cells were sorted into the (-) tube, and everything in between was not collected (Figure 1D). This more stringent sorted population was used for the Hi-C replicate presented in all Hi-C figures in the manuscript.

For flow cytometry experiments, cells were run on a BD LSR II (Clone ITGB4 expression levels, confluency and media depletion studies, and ITGB4(+) cells expression over time) or a Cytek Northern Lights flow cytometer (Sequential migration with flow and RNAi experiments). An Unstained population of cells was also used as a negative control to set a threshold value for ITGB4 expression. Cells were gated on real events, and doublets removed. To calculate the percentage of cells that express ITGB4, the percentage of events (cells) that had FITC (ITGB4) values over the Unstained condition were taken. Average ITGB4 intensity values are the average of the raw values of FITC collected by either flow cytometer for all cells in the condition. All analysis was done with Floreada.io (https://floreada.io).

Scratch assay

ITGB4(+), ITGB4(-), and Bottom10 cells were grown in single wells of a tissue culture treated 6-well plate to high confluency of ~90% in supplemented DMEM. Media was removed and each well was washed with 1mL of PBS. Scratch was made using a 10uL pipette tip by lightly applying pressure while moving along the bottom of the plate from bottom to top. Cells were then washed 3 times with unsupplemented DMEM to remove any debris. Finally, 1mL of DMEM supplemented with 0.1% FBS was added to the wells. Plates were then imaged for 24hr at 10min intervals using a 10x objective inside the live cell chamber of an EVOS II. Cells were kept at 37C, 5% CO2, and high humidity for the entirety of the image collection. Images were then stacked and turned into movies using Fiji Image Software.

3D collagen matrix

Experiments investigating the morphology and migration of A375 subpopulation of cells (ITGB4(+), ITGB4(-), and Bottom10) in 3D environment were performed using single cell suspension in 3D collagen matrices.[48] 75,000 cells/condition were added into collagen matrices (Rat Tail, Corning 354236) with a density of 2.32 mg/ml. The pH of the collagen gels was normalized to a neutral pH and gels were incubated at 37°C for 30 min to solidify. After the incubation, media with full supplements was supplied to the collagen gels. Cells were allowed to migrate through the collagen for 96hr before imaging.

Confluence and media depletion tests

To test the sensitivities of ITGB4 surface protein expression, Parental cells that had been through multiple rounds of migration were used. For Confluency, Parental cells that had made it through 4 rounds of migration were used. Cells from an 80% confluent 6-well plate were seeded at 15% and 50% density in 3mL of supplemented DMEM and allowed to proliferate for 24hr. The following day cells were ~30% and 95% confluent, respectively, and were stained for ITGB4 surface expression and run on a flow cytometer. For media influence, Parental cells through 4 rounds of migration were also used. Cells from an 80% confluent 6-well plate were seeded at 25% density in 3mL of supplemented DMEM in 2 wells and allowed to proliferate for 24hr. The following day, both wells had their media removed and replaced with either fresh supplemented DMEM, or media from a fully confluent well of a 6-well plate (depleted DMEM). The following day both wells were lifted and stained for ITGB4 surface protein expression and run on a flow cytometer. For combination treatments, Parental cells through 8 rounds of migration were used. Combination treatments followed the same procedures as described above.

ITGB4 RNAi

All supplies for siRNA experiments were ordered from Dharmacon. RNAi experiments were done following the manufacturers protocol in 24-well plates with final volumes of 500uL per well. Briefly, Human ITGB4 siRNA SMARTpool (L-008011-00-0005) and Non-targeting Pool (D-001810-10-05) were resuspended in 1x siRNA Buffer (B-002000-UB-100) to a final concentration of 5uM. 4 Eppendorf tubes were needed to create both the siRNA and the non-targeting control vectors. In the RNAi tube, 5uL of 5 μM ITGB4 siRNA was combined with 45uL of unsupplemented DMEM and mixed by pipetting and incubated at RT for 5 mins. Concurrently, the Non-targeting tube had 5uL of non-targeting RNAi mixed with 45uL of unsupplemented DMEM and incubated at RT for 5 mins. Also, 2 Eppendorf tubes containing 1uL of DharmaFECT 1 Transfection Reagent (T-2001-01) and 49uL of unsupplemented DMEM were mixed and incubated at RT for 5 mins. Following the incubation, RNAi and Non-targeting tubes were combined with a DharmaFECT tube (100uL total) and mixed by pipetting before incubating at RT for 20 minutes. Then, 400uL of antibiotic free DMEM (supplemented with 10% FBS, and 1% L-Glutamine) was added to each tube (500uL total). RNAi and Non-targeting transfection medias were then placed into respective wells containing 20,000 ITGB4(+) or Bottom10 cells and allowed to proliferate for 48hrs. After 48hr this process was repeated and fresh RNAi and Non-targeting transfection medias were given to the cells and another 48hr of proliferation occurred (96hr total). After 96hrs of exposure, 100,000 cells were placed into 5 μm pore Transwells to assess migration ability, and the remaining cells were run on a flow cytometer to assess ITGB4 surface protein expression. Non-transfected controls for both ITGB4(+) and Bottom10 cells were used to verify no expression knockdown occurred in the Non-targeting experiments.

Hi-C experiments

The first biological replicate of ITGB4 sorted cells was processed with the protocol described in (Golloshi et al., 2018). Briefly, 10 million cells were crosslinked with 1% formaldehyde for 10 min. Crosslinked cells were then suspended in lysis buffer to permeabilize the cell membrane and were dounce homogenized. Chromatin was then digested in-nucleus overnight using the DpnII restriction enzyme. Digested ends were filled in with biotin-dATP, and the blunt ends of interacting fragments were ligated together. DNA was then purified by phenol-chloroform extraction. For library preparation, the NEBNext Ultra II DNA Library prep kit (NEB) was used for libraries with size ranges from 200-400bp. End Prep, Adaptor Ligation, and PCR amplification reactions were carried out on bead-bound DNA libraries. All other Hi-C experiments were performed using the Arima-HiC+ Kit from Arima Genomics following the protocol for Mammalian Cell Lines (A160134 v01) and preparing the libraries using Arima recommendations for the NEBNext Ultra II DNA library prep kit (protocol version A16041v01). Sequencing was performed either through GeneWiz or at the UTK Genomics core using either an Illumina HiSeq or a Novaseq 6000 with 150bp paired end reads.

Hi-C data analysis

Sequencing reads were mapped to the human genome (hg19), filtered, and iteratively corrected by HiCPro (https://github.com/nservant/HiC-Pro). All Hi-C contact matrices were scaled to a sum of 1 million interactions to allow comparisons between conditions in downstream analysis. For library quality and mapping statistics, see Table S5.

Compartment analysis was performed by running principal component analysis using matrix2compartment.pl script in the cworld-dekker pipeline available on GitHub (https://github.com/dekkerlab/cworld-dekker). The PC1 value was then used to determine compartment identity for 250kb binned matrices. We considered PC1 values greater than 0.01 to be A compartment and less than −0.01 to be B compartment. To define compartment switches between conditions, PC1 values much go from positive to negative (A to B) or negative to positive (B to A). For compartment shifts between conditions, the difference between conditions had to have a PC1 value change greater than 0.04 (Towards A) or less than -0.04 (Towards B). This amount of PC1 change correlates with a 20% change in compartment score. Compartment profiles at specific genomic locations shown in figures are the result of the second replicate of ITGB4(+) and (-) Hi-C (resulting from the second, more stringent sort). For summary analyses (such as Figures 5E, 5F, and 6C), PC1 values from both replicates were averaged at each 250 kb bin. For clustering analysis, the top 200 most variable bins were used for compartment profile clustering.

Slope determination for shifted bins was completed as follows: Conditions were ordered from least to most migratory (i.e., Top-Unmigrated-Bottom10) and their PC1 values for all 250kb bins were determined. For each bin, the slope of the data points from least to most migratory was calculated and the bins were sorted from highest to lowest slope. Standard deviation of all slopes was calculated, and bins that had slopes ±1.5 standard deviations from the mean were considered for further analysis. Positive slopes were considered bins that shifted more towards the A compartment, whereas negative slopes were considered bins that shifted more towards the B compartment.

To determine genes within shifted or switched bins, the bins of interest were overlapped with the UCSC Genes ''knownGene'' track within genome hg19 and extracted for further analysis.

RNA-seq experiments

For all RNA-sequencing samples, RNA was extracted using the Qiagen RNAeasy plus mini kit. In short, cells were lysed and homogenized, spun down in gDNA eliminator columns to remove any genomic DNA. All samples were washed with ethanol, and the total RNA was eluted. The quality and quantity of the RNA were quantified using a nanodrop. Total RNA was then sent for library preparation (polyA mRNA approach) and sequencing at GeneWiz.

RNA-seq analysis

The fastq reads were first processed with BBDuk tool (https://github.com/kbaseapps/BBTools), performing adapter trimming. Adapter trimmed reads were processed for quality trimming using the BBDuk tool to discard reads with quality score lower than 28. Following the adapter and quality trimming steps, the reads were aligned to the reference genome hg19 using STAR aligner (https://github.com/alexdobin/STAR). Finally, the mapped reads were sorted based on genomic coordinates and feature count was performed with HTSeq-Counts (https://github.com/simon-anders/htseq). Differential gene expression was determined using DESeq through Galaxy. RNA-seq profile clustering was done by taking the 500 most variable genes throughout all conditions.

QUANTIFICATION AND STATISTICAL ANALYSIS

Unless otherwise indicated, GraphPad Prism was used to carry out statistical tests. Statistical details of each experiment (sample size, statistical tests used, definition of center and dispersion) are included in the figure legends. Sample size and replicate numbers for Transwell migration RNAi experiments were estimated by power analysis, using the calculator at https://sample-size.net/sample-size-means/ and the following parameters: alpha = 0.05, beta = 0.2, effect size to detect = 10% difference in migration, standard deviation = 7% of the mean. Transwell migration experiments were excluded from the final report if the total number of collected cells at the end of the experiment was 30% or more lower than the expected number (given the number of cells seeded into the well and known cell division rates).